

**EFFICIENT MODELING OF NUCLEI THROUGH COUPLING
OF PROTON AND NEUTRON WAVEFUNCTIONS**

A Thesis
Presented to the
Faculty of
San Diego State University

In Partial Fulfillment
of the Requirements for the Degree
Master of Science
in
Physics


by
Oliver Chauncey Gorton
Spring 2018

SAN DIEGO STATE UNIVERSITY

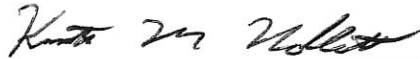
The Undersigned Faculty Committee Approves the

Thesis of Oliver Chauncey Gorton:

Efficient Modeling of Nuclei Through Coupling
of Proton and Neutron Wavefunctions



Calvin Johnson, Chair
Department of Physics



Kenneth Nollett
Department of Physics



Kate Rubin
Department of Astronomy

April 6, 2018
Approval Date

Copyright © 2018
by
Oliver Chauncey Gorton

DEDICATION

Dedicated to Grandpa David Basta.

ABSTRACT OF THE THESIS

Efficient Modeling of Nuclei Through Coupling
of Proton and Neutron Wavefunctions

by

Oliver Chauncey Gorton
Master of Science in Physics
San Diego State University, 2018

This thesis describes a nuclear shell model code which aims for a significant reduction in computer resource usage while retaining accuracy of results as compared to numerically exact solutions. I begin with an introduction to the configuration interaction and shell model calculations. I then motivate the need for a proton-neutron decomposition of the Hamiltonian, and present evidence for the viability of such a decomposition to reduce the size of the model space, through three different studies. The first is a series of calculations of proton-neutron entanglement entropy, a relatively novel approach in shell model calculations. Entanglement entropy measures the distribution of wavefunction coefficients, and thus the viability of truncation of a model space. These calculations study the strength and origin of the isospin dependence of the proton-neutron entanglement entropy. The second is a toy model that attempts to reproduce the entanglement entropy properties of realistic nuclear calculations. The third is a strength function decomposition of exact wavefunctions in an explicit proton-neutron formalism. Finally, I discuss a code to calculate nuclear wave-functions by a coupling of proton and neutron wave-functions which are calculated beforehand by an existing interacting shell model code. Results and convergence properties of this code are provided and discussed.

TABLE OF CONTENTS

	PAGE
ABSTRACT	v
LIST OF TABLES.....	viii
LIST OF FIGURES	ix
ACKNOWLEDGMENTS	xi
CHAPTER	
1 INTRODUCTION	1
Mathematical Background	2
Slater Determinants.....	4
Second Quantization.....	5
Effective Interactions and Shell Models	6
Bringing it All Together: the Interacting Shell Model	10
2 STATEMENT OF THE PROBLEM	13
Theoretical Motivation	14
Method	16
3 ENTANGLEMENT ENTROPY	17
Particle-Hole Conjugates	21
Excited States and Thermalization	23
Entropy and Isospin	23
Dialing the Strength of the Proton-Neutron Interaction	24
Modified Nuclear Interactions	26
Toy Model.....	28
Summary on Entanglement Entropy	35
4 PROTON-NEUTRON DECOMPOSITION	37
5 PNISM.....	41
The Hamiltonian	41
The Basis	43
Factorizing the Proton-Neutron Interaction	44

Matrix elements	47
One-body density matrices	48
6 COMPUTATION	51
Reading in Density Matrices	52
Symmetries	53
Numerical Methods	54
Challenges and Speedups	54
7 RESULTS	56
Capstone Calculations	57
Heavy Nuclei	58
8 CONCLUSION AND FUTURE WORK	64
REFERENCES	66
APPENDICES	
A Supplementary Notes	68
Vector Coupling Coefficients	69
3-j Symbol	69
6-j Symbols and 9-j Symbols	69
Singular Value Decomposition	69
Lanczos Method	70
Variational Principle	71
B Sample Density Matrix Files	73

LIST OF TABLES

Table 1. Harmonic Oscillator States with Spin Orbit Coupling	7
Table 2. <i>sd</i> -Shell Single Particle Orbits	9
Table 3. <i>pf</i> -Shell Single Particle Orbits	9
Table 4. <i>sd</i> -Shell Single-particle States	11
Table 5. Sample Shell Model Dimensions	13
Table 6. Table of Particle-Hole Conjugate Nuclei in the <i>sd</i> -Shell Model Space	22
Table 7. M-scheme Dimensions for Select Nuclei in the ($p_{1/2}$, $p_{3/2}$, $f_{5/2}$, $f_{7/2}$) Model Space.....	57
Table 8. Dimensions for Proton and Neutron Hamiltonians	57
Table 9. ^{56}Ni Ground State Energy and J-scheme Dimensions	58
Table 10. ^{60}Ni Ground State Energy and J-scheme Dimensions	58
Table 11. Estimated Dimensions of Target Heavy Nuclei.	59

LIST OF FIGURES

Figure 1. Normalized proton-neutron entanglement entropy for nuclei listed in Table 6. The horizontal axis labels particle-hole conjugate (PHC) triplets by the smallest nuclide in the leftmost column of Table 6 and are sorted left to right by increasing $S_{max} = \ln(\min[d_\pi, d_\nu])$. In most cases within each PHC triplet, the nuclide with an unequal numbers of protons and neutrons has the lowest entanglement entropy. All exceptions include nuclei with an odd-Z and odd-N (odd-odd) nuclide. (Circle: $N > Z$ nuclide, Square: heaviest PHC nuclide, Diamond: lightest PHC nuclide.)	23
Figure 2. Proton-neutron entanglement entropy versus excitation level for ^{28}Mg and its particle-hole conjugates in the sd -shell. The entanglement entropy is lower in the ^{28}Mg spectrum for the first ten excitation levels.	24
Figure 3. Entanglement entropy versus isospin for particle-hole conjugate nuclei in the sd -shell. Entanglement entropy tends to continuously decrease for even-even and even-odd numbers of protons and neutrons (see even-Z isotopes and even-N isotones), but to jump up for odd-odd nuclei (see odd-Z isotopes and odd-N isotones).....	25
Figure 4. Proton-neutron entanglement entropy as a function of the proton-neutron two-body interaction matrix element scaling factor λ . Entanglement entropy is necessarily zero when $\lambda = 0$. $\lambda < 0$ value are non-physical but shed light on the behavior of the coupling. ^{28}Ne , with an unequal number of protons and neutrons, has the lowest entanglement entropy for values of $\lambda > 0$ up until about seven times the realistic value of $\lambda = 1$	26
Figure 5. Entanglement entropy with a traceless interaction.	28
Figure 6. Entanglement entropy with an attractive quadrupole-quadrupole interaction.....	29
Figure 7. Attractive pairing interaction: Ne and PH-Conjugates.....	30
Figure 8. Random interactions exhibiting a bimodal distribution of entanglement entropy. No apparent correlation between entanglement entropy and ratio of protons to neutrons.....	31
Figure 9. Random traceless interactions exhibiting a unimodal distribution of entanglement entropy. No apparent correlation between entanglement entropy and ration of protons to neutrons. $N = Z$ nuclei have the same entanglement entropy for all interactions, as expected.	32

Figure 10. Toy Model with perturbative variance of the interaction W away from V . The subspaces containing the V interaction has the same dimensions as the subspace containing the W interaction. See equation (74).	33
Figure 11. Entanglement entropy S versus scaling factor λ for (a) toy model with non-separable two-body terms, and (b) nuclei in the pf -shell with a traceless interaction.	36
Figure 12. Strength decomposition of nuclear wavefunctions into eigenstates of the proton-proton or neutron-neutron interaction for two particle-hole conjugate nuclei in the sd -shell. Strengths fall off exponentially.	39
Figure 13. Strength decomposition of nuclear wavefunctions into eigenstates of the proton-proton or neutron-neutron interaction for two particle-hole conjugate nuclei in the sd -shell. The decomposition strengths of ^{28}Na , with an unequal number of protons and neutrons, fall off faster than its conjugate, suggesting that fewer states are necessary to represent it.	40
Figure 14. ^{22}Na low-lying excitation spectra as a function of n , the number of eigenstates retained from the pure proton and pure neutron interactions used to form the basis. Here the maximum value of n is $n = 37$, when the entire basis is retained.	60
Figure 15. ^{28}Na low-lying excitation spectra as a function of the number of retained n . $n_{max} = 37$. Notice that ^{28}Na converges faster than ^{22}Na , while having the same basis dimensions.	60
Figure 16. ^{24}Mg low-lying excitation spectra. Symbols as in Figure 14. Here $n_{max} = 81$	61
Figure 17. ^{28}Mg low-lying excitation spectra. Symbols as in Figure 14. $n_{max} = 81$ is the same as for ^{24}Mg , but energies converge faster for ^{28}Mg	61
Figure 18. ^{56}Ni ground state energy convergence relative to complete basis wavefunction.	62
Figure 19. ^{56}Ni low-lying excitation spectra. Unmarked curves are results from M-scheme calculation.	62
Figure 20. ^{60}Ni ground state energy convergence relative to complete basis wavefunctions as a function of the number of single-species basis states retained.	63
Figure 21. ^{60}Ni low-lying excitation spectra. Unmarked curves are results from M-scheme.	63

ACKNOWLEDGMENTS

I am grateful to my advisor and professor, Dr. Calvin Johnson, for guiding me through this, my first research project. His feedback and suggestions made this thesis better than it otherwise could have been. His instruction and our countless conversations and group meetings have enabled me to complete this research and to develop my scientific method. I would like to thank Dr. Kenneth Nollett and Dr. Kate Rubin for reviewing this manuscript and for their flexibility while serving on my committee. I also extend my thanks to my officemates for reading early drafts of my thesis and for listening to my presentation and offering their feedback.

CHAPTER 1

INTRODUCTION

Nuclear physics is the study of the structure and properties of atomic nuclei, which make up most of the known matter in the universe. The goal of nuclear theory is to make predictions about the interactions of nuclei with external fields, in order to answer questions about experimental outcomes and thereby related deeper and ongoing questions in physics about the fundamental symmetries of nature.

Some of the more important and open questions in physics, such as those related to the matter-antimatter symmetry violation, the source and origin of dark matter in the universe, and neutrinoless double beta decay, all rely on accurate and detailed quantum models of nuclei. Investigations into neutrinoless double beta decay call for transition matrix elements from ^{76}Ge and ^{76}Se .^{1,2} Some searches for dark matter involve collisions with heavy nuclei such as ^{131}Xe , and require detailed nuclear structure calculations.³ Finally, the origin of the matter-antimatter symmetry violation may be due to CP-violation,⁴ and one approach to investigating the source of CP-violation is through the permanent electric dipole moments of certain nuclei such as ^{199}Hg .⁵

In order to understand observations obtained from experiments, or to make predictions about future experiments, we need to be able to compute the matrix elements of operators with accurate nuclear wavefunctions computed from detailed Hamiltonians. I will be addressing the task of computing accurate wavefunctions from existing Hamiltonians, by solving the quantum N-body problem as a matrix eigenvalue problem. Because the complexity of many body problems scales exponentially with the number of particles, the dimension of these matrices can very large. This is especially true for medium and heavy nuclei. As a particular example, calculations of the parity violating nuclear “anapole moment” for nuclei such as ^{133}Cs and ^{205}Tl rely on accurate ground state wavefunctions, and one- and two-body density matrix elements.^{6,7} ^{133}Cs in the configuration interaction shell model, a kind of matrix eigenvalue problem, has a basis dimension of over one-hundred million and

requires nearly 800 GB of memory to store just the non-zero matrix elements of the Hamiltonian. Given the enormity of such problems and finite computer memory, it becomes of interest to find ways to reduce the size of such matrices. In principle, this can be done by truncating the basis and computing only the matrix elements whose basis elements are most important. In this thesis I will present in considerable detail evidence that this is a plausible strategy in a specific framework for our choice of basis. Furthermore, I will present evidence that this should work *better* for the kinds of cases we will face for medium and heavy nuclei, that is, with unequal numbers of protons and neutrons.

The framework that we will work in is a proton-neutron coupling scheme, the details of which will be discussed in Chapter 5. The evidence will be the *entropy of entanglement* between protons and neutrons in atomic nuclei, which I will use to show that one can, in principle, efficiently truncate the basis. The question of *how* this can actually be done is still under investigation. I will present, however, a code which carries out the coupling and give our results to date. While the project of efficiently calculating nuclear properties using a truncated basis is not yet complete, I can demonstrate significant progress towards it.

MATHEMATICAL BACKGROUND

In this and the following section I give a brief introduction to the mathematical underpinning of the nuclear many body problem. I assume an understanding of undergraduate quantum mechanics.

Nuclear physics is essentially a quantum many-body problem and much of nuclear physics can be explained by the (non-relativistic) N-body Schrödinger equation:

$$\hat{H}\Psi(\vec{r}_1, \vec{r}_2, \vec{r}_3, \dots, \vec{r}_N) = E\Psi(\vec{r}_1, \vec{r}_2, \vec{r}_3, \dots, \vec{r}_N). \quad (1)$$

Here \hat{H} is the Hamiltonian, which includes kinetic energy and potential energy terms for each particle. The potential energy contains the nuclear interaction and/or other relevant interactions like the Coulomb force.⁸ Ψ is our wave-function, a function of the position of every particle in the system. If we could solve the Schrödinger equation for every system, the task of the theoretical nuclear physicist would be complete. However, in general, there is no analytic solution to (1) except for in a very small number of cases involving a great deal of symmetry and a small number of particles. In any practical situation where calculations of realistic nuclear structure are required, numerical methods are necessary.

Towards this end, let's review the matrix formulation of quantum mechanics. Let us start with an eigenvalue equation of the form

$$\hat{H}|\Psi\rangle = E|\Psi\rangle. \quad (2)$$

\hat{H} is a Hermitian operator on a Hilbert space \mathcal{H} and $|\Psi\rangle$ is a state vector which is a member of the Hilbert space. (A Hilbert space is a vector space with an inner product that is complete in the norm).⁹ By definition, any basis $\{|\alpha\rangle\}$ must satisfy the completeness relation

$$1 = \sum_{\alpha} |\alpha\rangle\langle\alpha|, \quad (3)$$

thus any state vector $|\Psi\rangle$ can be expressed as the following, where $\Psi_{\alpha} \equiv \langle\alpha|\Psi\rangle$

$$|\Psi\rangle = \sum_{\alpha} \Psi_{\alpha} |\alpha\rangle. \quad (4)$$

For this to be meaningful we will eventually need to choose a particular basis to work in. Starting again from (2) and substituting this representation of our eigenstate,

$$\hat{H} \sum_{\alpha} \Psi_{\alpha} |\alpha\rangle = E \sum_{\alpha} \Psi_{\alpha} |\alpha\rangle \quad (5)$$

and projecting onto a dual basis state $\langle\beta|$

$$\begin{aligned} \langle\beta|\hat{H} \sum_{\alpha} \Psi_{\alpha} |\alpha\rangle &= \langle\beta|E \sum_{\alpha} \Psi_{\alpha} |\alpha\rangle \\ \sum_{\alpha} \langle\beta|\hat{H}|\alpha\rangle \Psi_{\alpha} &= \sum_{\alpha} \langle\beta|\alpha\rangle E \Psi_{\alpha} \\ \sum_{\alpha} H_{\beta\alpha} \Psi_{\alpha} &= E \Psi_{\beta}, \end{aligned} \quad (6)$$

where the matrix elements of \hat{H} are defined to be

$$H_{\beta\alpha} \equiv \langle\beta|\hat{H}|\alpha\rangle. \quad (7)$$

Now that we have represented the Schrodinger equation as a matrix eigenvalue problem, it becomes in principle straightforward to obtain important results such as the energy spectra and transition probabilities of nuclei: simply diagonalize the Hamiltonian matrix to obtain the energy spectrum (eigenvalues) and wavefunctions (eigenvectors), which are used to compute observables such as transition probabilities.

Complications include the fact there is really no way to write down a simple analytic Hamiltonian for the nuclear force as there is for classical forces such as electromagnetism. The nuclear force is fundamentally an exchange of mesons requiring quantum field theory to properly describe.¹⁰ Furthermore, even once a Hamiltonian is obtained, solving for its eigenvalues can be a non-trivial computational problem, since the dimensions of the space can be in the many-billions. There are a number of popular computational methods for solving the many-body Hamiltonian, of which the configuration interaction method is an example.

SLATER DETERMINANTS

A common practice in the configuration interaction model is to write the many-body basis states $\{|\alpha\rangle\}$ used above in terms of anti-symmetrized products of single-particle solutions to a single-particle Hamiltonian. Let's explore what this means.

Because our wavefunctions Ψ live in a vector space (more precisely, in a Hilbert space) we can always rewrite Ψ in another basis of our choosing.

$$\Psi(\vec{r}_1, \vec{r}_2, \vec{r}_3, \dots, \vec{r}_N) = \sum_{\alpha} c_{\alpha} \Phi_{\alpha}(\vec{r}_1, \vec{r}_2, \vec{r}_3, \dots, \vec{r}_N) \quad (8)$$

This is an N -body wavefunction with N sets of coordinates, one for each particle. The CI method is to choose our Φ to be a product of single-particle wave functions,

$$\{\phi_a\}, \quad a = 1, \dots, d, \quad (9)$$

where d is the number of single-particle states. These single-particle wavefunctions are chosen to be some convenient basis that will span the Hilbert space of interest. I will discuss the exact nature of the single-particle states in Section 1.4. The normalization integral of a product wavefunction is simply the product of the integrals of each factor. However, since nuclei are composed of fermions (spin-1/2 particles), we must have antisymmetric wavefunctions. We therefore need the more complicated rule:¹¹

$$\Phi(\vec{r}_1, \vec{r}_2, \vec{r}_3, \dots, \vec{r}_N) = \frac{1}{\sqrt{N!}} \sum_{i_1, i_2, \dots, i_N}^N \epsilon_{i_1, i_2, \dots, i_N} \phi_1(\vec{r}_{i_1}) \phi_2(\vec{r}_{i_2}) \phi_3(\vec{r}_{i_3}) \dots \phi_d(\vec{r}_{i_N}), \quad (10)$$

viz. the determinant of the matrix defined by $[\phi_a(i_b)]$ with a normalization factor, with index a labeling the single-particle state and index i_b labeling the particle number. The antisymmetry is encoded in the Levi-Civita symbol $\epsilon_{i_1, i_2, \dots, i_N}$.¹² By defining our many-body wave-functions

to be determinants of single-particle wavefunctions we are guaranteed antisymmetric many-body states. These specially constructed states are known as Slater determinants.¹³

SECOND QUANTIZATION

Occupation representation is an additional formalism that is used in our representation of wavefunctions. Here I will only state the relevant results of this so-called second quantization formalism. Many-body basis states are no longer represented as the product of coordinate functions of single particle states. Instead, a basis of single-particle states is chosen, perhaps the same set $\{\phi_a\}$ as above, and the many-body states are represented in the abstract as

$$\Psi(\vec{r}_1, \vec{r}_2, \vec{r}_3, \dots, \vec{r}_N) \rightarrow \Psi\{n_\phi\} = |n_1, n_2 \dots n_d\rangle, \quad (11)$$

where n_a is the number of particles in the state ϕ_a . Without any additional structure, this representation lacks anti-symmetry; this is restored by representing the state $|n_1, n_2 \dots n_d\rangle$ as the action of a series of operators on the vacuum state $|0, 0 \dots 0\rangle$, or “particle vacuum”. The operator which turns $|0, 0 \dots 0\rangle$ into $|1, 0 \dots 0\rangle$ is called the creation operator, and the operator which turns $|1, 0 \dots 0\rangle$ into $|0, 0 \dots 0\rangle$ is called the annihilation operator. For fermions, these two generalized ladder operators are defined implicitly through their anti-commutation relations:¹⁴

$$\begin{aligned} \{\hat{a}_i, \hat{a}_j^\dagger\} &\equiv \hat{a}_i \hat{a}_j^\dagger + \hat{a}_j^\dagger \hat{a}_i = \delta_{ij} \\ \{\hat{a}_j, \hat{a}_j\} &= \{\hat{a}_i^\dagger, \hat{a}_j^\dagger\} = 0 \end{aligned} \quad (12)$$

These anti-commutation relations encode the properties of systems of fermions: two fermions cannot occupy the same state, $(\hat{a}_i^\dagger)^2 = 0$, and therefore the maximum occupancy of a state ϕ_i is one. Thus,

$$\begin{aligned} \hat{a}_1^\dagger |1, 0, \dots, 0\rangle &= 0, \\ \hat{a}_1^\dagger |0, 0, \dots, 0\rangle &= |1, 0, \dots, 0\rangle, \\ \hat{a}_1 |1, 0, \dots, 0\rangle &= |0, 0, \dots, 0\rangle, \\ \hat{a}_1 |0, 0, \dots, 0\rangle &= 0, \end{aligned} \quad (13)$$

and so on for any state $|n_1, n_2 \dots n_d\rangle$. With this mathematically equivalent structure, we can replace our Slater determinants (10) with occupation representations using second quantization operators. Any many body state can now be written

$$\Phi = |n_1, n_2 \dots n_d\rangle = (\hat{a}_1^\dagger)^{n_1} \dots (\hat{a}_d^\dagger)^{n_d} |0, \dots, 0\rangle. \quad (14)$$

Since each state's occupation n_i is constrained to 0 or 1, many body states can be represented by bit strings. For example,¹⁵

$$\hat{a}_1^\dagger \hat{a}_4^\dagger \hat{a}_5^\dagger \hat{a}_7^\dagger |0\rangle = |1457\rangle \Rightarrow 1001101, \quad (15)$$

where we are dealing with a four-body wavefunction in a basis with at least seven single-particle states, and where I have used $|0\rangle$ here in place of $|0, \dots, 0\rangle$ for brevity. This makes computer storage of wavefunctions trivial.

It can be shown that one-body operators can be expressed in the second quantization formalism as:¹⁶

$$\hat{O} = \sum_{ij} \langle i|O|j\rangle \hat{a}_i^\dagger \hat{a}_j, \quad (16)$$

where the sum is over all single-particle states. Similarly, two-body operators can be expressed:¹⁶

$$\hat{O} = \frac{1}{4} \sum_{ijkl} \langle ij|O|kl\rangle \hat{a}_i^\dagger \hat{a}_j^\dagger \hat{a}_k \hat{a}_l. \quad (17)$$

The factor of one-fourth comes from the fact that the sum is over all single-particle states and would otherwise over count the number of (pairwise) interactions. The Hamiltonian may be rewritten using these representations:

$$\hat{H} = \sum_{i,j} \hat{a}_i^\dagger \langle i|T|j\rangle \hat{a}_j + \frac{1}{4} \sum_{i,j,k,l} \hat{a}_i^\dagger \hat{a}_j^\dagger \langle ij|V|kl\rangle \hat{a}_l \hat{a}_k, \quad (18)$$

where the first term represents the one-body interactions such as kinetic energy or the Coulomb interaction with an external field, and the second term represents two-body interactions (forces between interacting particles) and contains the nuclear force. This formalism is key to the way this model is translated into powerful computer codes which can be used for a number of different calculations.

EFFECTIVE INTERACTIONS AND SHELL MODELS

A truly realistic model of the nucleus would necessarily involve the description of the exchange of mesons.¹⁰ The basis of single particle states $\{\phi_a\}$ that are used in shell model methods are instead taken to be time independent solutions to quantum potentials which attempt to reproduce the results of a full field theory. Some variation of a mean-field approximation is used to motivate the choice of single particle states. For example, this could be a harmonic oscillator, or the more sophisticated Woods-Saxon potential.¹⁶ In both cases,

and in all cases considered here, the defining single-particle potential is chosen to exhibit rotational invariance, resulting in states of good angular momentum. In fact we will always choose single particle states with good harmonic oscillator quantum numbers: the radial quantum number n , the orbital angular momentum l , the total angular momentum j , the z-component of the angular momentum $j_z \equiv m$ and the parity quantum number π . Parity $\pi = (-1)^l$ and $m = -j, -j + 1, \dots, j - 1, j$.

It is common practice to use atomic spectroscopic notation to label the nuclear single-particle orbits (states). Here we will take the convention nl_j where l is replaced with the letters

$$\begin{aligned} l &= 0, 1, 2, 3, 4, 5, \dots \\ &= s, p, d, f, g, \dots \end{aligned} \tag{19}$$

For example the first few low-lying levels of a harmonic oscillator-like single-particle potential are shown in Table 1. (Degeneracy indicates the numbers of states with unique m in each orbit nl_j . Max fill indicates the sum of all degeneracies up to that orbit and is the maximum number of nucleons of each species that can fill the space up to and including that orbit.). There is a distinction between an orbit nl_j and a state which also includes the z-component of the angular momentum m . An orbit labeled as nl_j has $2j + 1$ possible states since m is restricted to $-j, -j + 1, \dots, j - 1, j$. States within the same orbit are degenerate in energy (at least in the absence of any external electromagnetic fields), with $2j + 1$ being the degeneracy.

Table 1. Harmonic Oscillator States with Spin Orbit Coupling

Orbit	n	l	j	m	Parity	Degeneracy	Max fill
$0s_{1/2}$	1	0	$1/2$	$1/2, -1/2$	+	2	2*
$1p_{3/2}$	1	1	$3/2$	$3/2, \dots, -3/2$	-	4	6
$1p_{1/2}$	1	1	$1/2$	$1/2, -1/2$	-	2	8*
$1d_{5/2}$	1	2	$5/2$	$5/2, \dots, -5/2$	+	6	14
$2s_{1/2}$	2	0	$1/2$	$1/2, -1/2$	+	2	16
$1d_{3/2}$	1	2	$3/2$	$3/2, \dots, -3/2$	+	4	20*
$1f_{7/2}$	1	3	$7/2$	$7/2, \dots, -7/2$	-	8	28*
$2p_{3/2}$	2	1	$3/2$	$3/2, \dots, -3/2$	-	4	32
$1f_{5/2}$	1	3	$5/2$	$5/2, \dots, -5/2$	-	6	38
$2p_{1/2}$	2	1	$1/2$	$1/2, -1/2$	-	2	40
$1g_{9/2}$	1	4	$9/2$	$9/2, \dots, -9/2$	+	10	50*

In the harmonic oscillator basis, there are an infinite number of single-particle states. We cannot keep track of an infinite number of states; this would require bit string representations of our many-particle states that are infinitely long. We therefore consider only a finite number of single-particle states, and leave out the rest. We leave out single-particle states which have a very low probability of being occupied, as well as those with a very high occupation probability. This second statement may seem counter-intuitive. How can we ignore states which are occupied? Because these states are assumed to always be occupied, we can account for their contribution to the single-particle energies and two-body interactions while leaving the states out of the active model space. To determine which low-lying states are likely to always be filled, we rely on “magic numbers”. An important observational fact is that the binding energy of certain nuclei with certain numbers of nucleons tend to be especially stable. Nuclei with 2, 8, 20, 28, 50, 82, or 126 protons or neutrons tend to have a higher binding energy than nuclei with one proton or one neutron above these so called magic numbers.¹⁷ Magic numbers in Table 1 are marked with an asterisk.

In shell model codes, the vacuum state is redefined to be an inert core of nucleons, and the model space to be a finite space of particle-hole excitations near a Fermi surface,¹⁸ usually determined by one of the magic numbers. Particles in the set of active, interacting nuclei occupy the “valence” space. For example, we can imagine an inert core of 8 noninteracting protons and 8 noninteracting neutrons, which can be thought of as a frozen ^{16}O nucleus. Then, orbiting above this core we can imagine a fixed number of interacting nucleons, valence protons and neutrons. If we restrict the number of valence protons and neutrons to between 0 and 12, then we can represent the entire valence space with just the $d_{3/2}$, $d_{5/2}$ and $s_{1/2}$ orbitals. This is called the sd -shell model space because the $s(l = 0)$ and $d(l = 2)$ orbital quantum numbers are all that appear in the truncated model space. All quantum numbers for this single-particle model space are shown in Table 2. (These orbits lie directly above an inert core of 8 protons and 8 neutrons and can support up to 12 valence protons and 12 valence neutrons. Each orbit has $2j + 1$ possible values of m , this is the degeneracy. The rightmost column indicates the maximum number of particles that could fill the model space up to that orbit.) The overall effect of the inert ^{16}O core is to add an effective energy to Hamiltonian.¹⁸

Another common space that we will be using is the $f_{7/2}$, $p_{3/2}$, $f_{5/2}$, and $p_{1/2}$ model space, often referred to as the pf -shell model space. The single-particle orbits for this space

Table 2. *sd*-Shell Single Particle Orbits

Orbit	l	j	m	Degeneracy	Max fill
$d_{3/2}$	2	3/2	3/2, 1/2, -1/2, -3/2	4	4
$d_{5/2}$	2	5/2	5/2, 3/2, 1/2, -1/2, -3/2, -5/2	6	10
$s_{1/2}$	0	1/2	1/2, -1/2	2	12

are given in Table 3. (Same conventions as in Table 2. This model space has an inert core of 20 protons and 20 neutrons and has 20 unique proton and 20 unique neutron states.)

Table 3. *pf*-Shell Single Particle Orbits

Orbit	n	l	j	m	Degeneracy	Max fill
$1f_{7/2}$	1	3	7/2	7/2, ..., -7/2	8	8
$2p_{3/2}$	2	1	3/2	3/2, 1/2, -1/2, -3/2	4	12
$1f_{5/2}$	1	3	5/2	5/2, ..., -5/2	6	18
$2p_{1/2}$	2	1	1/2	1/2, -1/2	2	20

To account for the state left out of the model space, an effective two-body interaction can be computed. By enforcing that the effective interaction acting on the model wavefunction reproduces the same results as the full interaction on the full wavefunction, one can expand the effective interaction into a series of the form¹⁸

$$V^{eff} = V + V \frac{\hat{Q}}{E - H_0} V + \dots \quad (20)$$

where \hat{Q} is a projection operator onto the part of the full Hilbert space that was left out of the model.

In our work we rely on commonly used effective two-body interactions computed by others, such as the Universal *sd*-shell interaction version B (USDB).¹⁹ This interaction is not derived using an expansion like (20), however. The USDB interaction and others like it are phenomenological interactions, meaning that it may have started from an effective calculation like equation (20), but then matrix elements were tuned in order to give better fits to widely available measured masses and resonance energies (e.g. from the National Nuclear Data Center (NNDC)).²⁰ The USDB interaction and other widely used interaction matrix elements are lists of quantities of the form

$$\langle i, j | V | k, l \rangle, \quad (21)$$

as appears in equation (18).

BRINGING IT ALL TOGETHER: THE INTERACTING SHELL MODEL

To construct a many-body basis in the interacting shell model, we begin with a shell model space. I will use the *sd*-shell model space to illustrate the development of this section. This model space has an inert core of 8 protons and 8 neutrons. The contribution from these inactive particles is accounted for in the single-particle energies and two-body matrix elements of the Hamiltonian. We have three single particle orbits ($d_{3/2}$, $d_{5/2}$, and $s_{1/2}$), each with a $2j + 1$ degeneracy. We often assume that protons and neutrons have the same set of single-particle orbits. Each orbit has a single-particle energy associated with it. Given the degeneracy of each orbit, we have 12 possible single-particle states, as shown in Table 4. These single-particle states span the valence space, that is, the space of all possible single-particle wavefunctions within the *sd*-shell model space. Many-particle wavefunctions, i.e. proton or neutron Slater determinants, can be represented with a bit string twelve bits long. If there are N fermions of a given species in the model space, then there are ${}_{12}C_N$ (twelve choose N) possible Slater determinants. For example, a state with three protons (or neutrons) could be

$$\hat{a}_1^\dagger \hat{a}_2^\dagger \hat{a}_3^\dagger |0\rangle = |123\rangle = |111000000000\rangle \rightarrow 111000000000, \quad (22)$$

but there are ${}_{12}C_3 = 220$ possible 3-nucleon Slater determinants, many of them degenerate in energy. The single-particle energy of such a state (i.e. ignoring nucleon-nucleon interactions) would be the sum of the single-particle energies of each nucleon.

Equation (22) is a many-proton or many-neutron Slater determinant. The wavefunction of an atomic nucleus, containing both protons and neutrons, is constructed by coupling together proton and neutron Slater determinants:

$$|\alpha\rangle = |j_p, m_p\rangle \otimes |j_n, m_n\rangle, \quad (23)$$

where $|j_p, m_p\rangle = (\hat{a}_1^\dagger)^{n_1} \dots (\hat{a}_d^\dagger)^{n_d} |0, \dots, 0\rangle$ is a particular proton Slater determinant such as (22), and similarly for the many-neutron state $|j_n, m_n\rangle$.

The number of nuclear Slater determinants can quickly become very large. The *sd*-shell model space, with 12 single-particle states, has a maximum of ${}_{12}C_6 = 924$ single-species Slater determinants, for a maximum of $924^2 = 853776$ proton-neutron Slater determinants. Fortunately, symmetries of the Hamiltonian, specifically selection rules for

Table 4. *sd*-Shell Single-particle States

State #	Orbit	l	π (Parity)	j	m
1	$d_{3/2}$	2	+	3/2	+3/2
2	$d_{3/2}$	2	+	3/2	+1/2
3	$d_{3/2}$	2	+	3/2	-1/2
4	$d_{3/2}$	2	+	3/2	-3/2
5	$d_{5/2}$	2	+	5/2	+5/2
6	$d_{5/2}$	2	+	5/2	+3/2
7	$d_{5/2}$	2	+	5/2	+1/2
8	$d_{5/2}$	2	+	5/2	-1/2
9	$d_{5/2}$	2	+	5/2	-3/2
10	$d_{5/2}$	2	+	5/2	-5/2
11	$s_{1/2}$	0	+	1/2	+1/2
12	$s_{1/2}$	0	+	1/2	-1/2

quantum numbers allow us to ignore certain combinations of these states, allowing us to reduce the overall size of the basis. If the Hamiltonian is rotationally invariant, then both the total angular momentum operator \hat{J}^2 and the z-component of angular momentum operator \hat{J}_z commute with the Hamiltonian. This makes choices of basis where either J or $J_z = M$ is held constant for all basis states convenient,⁸ since for any coupled basis states $|\alpha, M_j\rangle$ with good total M

$$\langle\beta, M_\beta|\hat{H}|\alpha, M_\alpha\rangle = 0, \quad (24)$$

whenever $M_\alpha \neq M_\beta$. This holds true for states of fixed J as well, but in general this is less convenient because whereas M is an additive quantum number, J is not and requires more cumbersome combinations of Slater determinants.⁸ Therefore for (23) we often choose the so-called M-scheme basis where basis states are coupled up to good M :

$$|\alpha\rangle = [|j_p m_p\rangle \otimes |j_n m_n\rangle]_M \equiv |j_p j_n; M\rangle, \quad (25)$$

where $M = m_p + m_n$. In terms of our bit representations this means selecting to combine proton Slater determinants with neutron Slater determinants that will result in fixed total M . For example, an atomic nucleus in the *sd*-shell model space with a single valence proton and a

single valence neutron (i.e. ^{18}F) for $M = 0$ can only have coupled Slater determinants such as

$$\begin{aligned}
 |1\rangle \otimes |4\rangle &= |j_p = 3/2, m_p = +3/2\rangle \otimes |j_n = 3/2, m_n = -3/2\rangle, \\
 |4\rangle \otimes |1\rangle &= |j_p = 3/2, m_p = -3/2\rangle \otimes |j_n = 3/2, m_n = +3/2\rangle, \\
 |2\rangle \otimes |3\rangle &= |j_p = 3/2, m_p = +1/2\rangle \otimes |j_n = 3/2, m_n = -1/2\rangle, \\
 |3\rangle \otimes |2\rangle &= |j_p = 3/2, m_p = -1/2\rangle \otimes |j_n = 3/2, m_n = +1/2\rangle,
 \end{aligned} \tag{26}$$

etc., where $|i\rangle$ is a single particle occupying the i^{th} single-particle state in Table 4. In total there are 28 possible $M = 0$ coupled Slater determinants for ^{18}F in the sd -shell model space, translating to a basis and Hamiltonian matrix with a dimension of 28.

The M-scheme is highly advantageous. However, if we wish to truncate the basis, the J-scheme becomes preferable. I will explain this in detail in a later chapter, after justifying the need for a truncation of the basis.

CHAPTER 2

STATEMENT OF THE PROBLEM

In order to solve the nuclear many-body problem, the Schrodinger equation is recast as a matrix eigenvalue problem. We use an M-scheme configuration interaction code called BIGSTICK^{8, 15}. Despite the fact that the interaction files used to build the basis for the space are semi-empirical, BIGSTICK and codes like it are still numerically exact, that is, they don't use any numerical approximations once the Hamiltonian is built, and the basis is not truncated. This means that the error relative to experiment is due to the interaction the code uses and not the method for solving the problem. The error in the results are fairly low, around a few hundred keV, while low-lying states tend to be a few MeV in magnitude. BIGSTICK and configuration interaction codes like it can still be extremely computationally expensive to run for large nuclei, even after an order of magnitude improvement using the M-scheme. Table 5 contains a short list of the storage space (RAM) required to store just the nonzero matrix elements for various nuclei in different phenomenological model spaces. A discussion of the dimensions of even heavier nuclei can be found in Chapter 7.

Table 5. Sample Shell Model Dimensions

Nuclide	Space	Basis dim.	Storage ^{8,15} (GB)
²⁸ Si	<i>sd</i>	9.4×10^4	0.2
⁵² Fe	<i>pf</i>	1.1×10^8	720
⁵⁶ Ni	<i>pf</i>	1.1×10^9	9600

Because of the intense computational cost of solving nuclear structure problems, and the limited computer resources available, it is necessary to approximate solutions via truncated model spaces. The purpose of this thesis is to investigate the viability of truncating the nuclear many-body basis in a particular framework, a basis of coupled proton and neutron Slater determinants, and to truncate the basis by selecting the most important states. The best method for doing so has yet to be determined, but later in Chapter 5 I will explain the attempt we have made. First I will provide evidence that such a method could be viable.

To do so I analyze the distribution of wavefunction coefficients. This investigation was inspired by a similar study of light to medium mass nuclei using a singular value decomposition (SVD) of the wavefunction coefficients.^{21–23} In those studies, shell model basis states were approximated by truncating the basis in a coupled proton-neutron scheme. Ground state energies in the *sd* and *pf* shell, as well as low-lying states, were shown to converge exponentially with basis dimension to those computed with the untruncated basis. The authors examined mostly $N = Z$ nuclei. The authors also provided no explanation for the cause of the exponential convergence, and restricted themselves to relatively low dimensional problems. In the next chapter, I will take a similar approach by examining the distribution of wavefunction coefficients through the proton-neutron entanglement entropy.

THEORETICAL MOTIVATION

We can always expand a wavefunction into any basis. Suppose we have some initial representation of our wavefunction,

$$|\Psi\rangle = \sum_{i_p, j_p} \Psi_{i_p, j_p} |i_p\rangle |j_p\rangle, \quad (27)$$

where the uncoupled basis states are Slater determinants:

$$|i_p\rangle \text{ and } |j_p\rangle, \quad (28)$$

where $i_p = 1, d_p$ and $j_p = 1, d_n$. Here, d_p and d_n are the number of proton and neutron basis states, respectively.

We choose to decompose our wavefunction $|\Psi\rangle$ into pure proton $|\pi_a\rangle$ and pure neutron $|\nu_b\rangle$ wavefunctions which are related to the old basis by some unitary transformation,

$$|\pi_a\rangle = \sum_{i_p} U_{ai_p}^\pi |i_p\rangle, \quad (29)$$

and similarly for $|j_p\rangle$ and $|\nu_b\rangle$. Thus we can find

$$|\Psi\rangle = \sum_{a,b} \tilde{\Psi}_{ab} |\pi_a\rangle |\nu_b\rangle, \quad (30)$$

where a enumerates proton single-particle states and b enumerates neutron single-particle states. If the sum is taken over all states, (30) is equivalent to (27). The goal, however, is to find a basis in which the sum (30) can be truncated, thus reducing the size of the problem.

$$|\Psi\rangle = \sum_{a,b=1}^N \tilde{\Psi}_{ab} |\pi_a\rangle |\nu_b\rangle, \quad N \ll \min(d_p, d_n). \quad (31)$$

In order for the truncated sum to be useful, the terms we exclude must be small compared to the overall wavefunction. If we have some normalized representation of a wavefunction,

$$|\Psi\rangle = \sum_{\alpha} c_{\alpha} |\Phi_{\alpha}\rangle, \quad (32)$$

then the sum of the weights $|c_{\alpha}|^2$ is unity:

$$1 = \sum_{\alpha} |c_{\alpha}|^2, \quad (33)$$

and the distribution of the weights $|c_i|^2$ tells us how much the sum (32) can be truncated in the basis $|\Phi_i\rangle$.

In a basis of coupled single particle states as in (27), the coefficients form a non-symmetric matrix Ψ_{i_p, j_n} . However, it was shown in the studies cited above^{21–23} that a singular value decomposition²⁴ (SVD) of this matrix would transform Ψ_{i_p, j_n} into a diagonal matrix such that

$$|\Psi\rangle = \sum_i \gamma_i |\tilde{i}_p\rangle |\tilde{i}_n\rangle, \quad (34)$$

where $\gamma_i = \tilde{\Psi}_{ii}$ are the diagonal elements of the transformed matrix of Ψ_{i_p, j_n} , and $|\tilde{i}_p\rangle$ and $|\tilde{i}_n\rangle$ are some undetermined basis states. (See Appendix A.4 or Chapter 3 for a more detailed explanation of singular value decompositions.) If such an expansion could be found, then, as for the simple case in (32), the distribution of expansion coefficients γ_i would tell us how much the expansion (34) could be truncated. The problem of course is determining the best basis, an as-yet unsolved problem. Nonetheless, there is still something to be learned from singular value decompositions. Just as eigenvalues are invariant under a change of basis, the “eigenvalues” γ_i are also invariant under a change of basis. (In fact these SVD eigenvalues and the SVD itself are generalizations of eigenvalue decompositions.) Therefore, we can compute the SVD eigenvalues of a known expansion, such as from the nuclear wavefunctions from an M-scheme method (e.g. BIGSTICK), and at the very least we can determine whether or not an truncation is possible.

METHOD

I conduct two related studies: In Chapter 3, I will examine the distribution of nuclear wavefunction amplitudes, from which we extract the proton-neutron entanglement entropy. I provide evidence that the creation of approximate wavefunctions through coupling of proton and neutron wavefunctions may be a valuable method, and I test a postulate which predicts that this proton-neutron coupling scheme will be even more effective for nuclei where the number of neutrons is much larger than the number of protons, i.e. for large isospin. Chapter 3 also attempts to investigate the cause of this behavior via the entanglement entropy. Then in Chapter 4, I will decompose BIGSTICK wavefunctions into their pure-proton and pure-neutron components by projecting the existing wavefunctions onto the appropriate operators. This, I will argue, demonstrates directly that a truncated basis of coupled proton and neutron Slater determinants can accurately reproduce nuclear wavefunctions.

CHAPTER 3

ENTANGLEMENT ENTROPY

In this chapter I will explain in detail the method we will use to generate evidence our nuclear wavefunctions can be significantly truncated. We will use the entanglement entropy of protons and neutrons (the entropy of entanglement between protons and neutrons) to do this.

The entanglement entropy is a way to quantify the distribution of wavefunction coefficients. Entanglement entropy pertains to bipartite systems, Hilbert spaces with more than one species of wavefunction that can be represented as an outer product of two or more subsystems. For us this means that our total Hilbert $\mathcal{H}^{\pi\nu}$ is the outer product of the subspace of many-proton states \mathcal{H}_π with the subspace of many-neutron states \mathcal{H}_ν :

$$\mathcal{H}^{\pi\nu} = \mathcal{H}_\pi \otimes \mathcal{H}_\nu. \quad (35)$$

This is congruent with the fact that our basis states are written as outer products of proton and neutron Slater determinants. It will be shown that a wavefunction with zero proton-neutron entanglement entropy can be written with a single term in an expansion such as (34). To do this I will first explain how the proton-neutron entanglement entropy comes naturally out of a singular value decomposition of the coefficients of a wavefunction in a basis of coupled proton and neutron wavefunctions.

A singular value decomposition is a factorization of any matrix A into the following form:

$$A = UDV^\dagger, \quad (36)$$

where U and V are unitary matrices and D is a diagonal matrix. The diagonal elements of D are the SVD eigenvalues. See Appendix A.4 for more information about singular value decompositions. The matrices don't have to be square. Notice that if we compute AA^\dagger we find:

$$\begin{aligned} AA^\dagger &= UDV^\dagger(UDV^\dagger)^\dagger \\ &= UDV^\dagger V D^\dagger U^\dagger \\ &= UDD^\dagger U^\dagger, \end{aligned} \quad (37)$$

where now $D^\dagger D = D^2$ is diagonal, square, and positive definite. The SVD eigenvalues γ_i can thus be obtained from the diagonal elements γ_i^2 of D^2 by diagonalizing AA^\dagger . Since equation (37) represents a unitary transformation of a matrix, the SVD eigenvalues are invariant. This means that the SVD eigenvalues of the coefficients in the expansion (31) can be found by diagonalizing the matrix

$$(AA^\dagger)_{a'a} = \sum_b \Psi_{a'b} \Psi_{ba}^*, \quad (38)$$

from the coefficients in equation (27) which we can find from solutions in a known basis.

Equation (38) is simply the reduced density matrix of the eigenstate $|\Psi\rangle$ in the choice of basis given in (27). The *density operator* of a pure state Ψ is defined as

$$\rho = |\Psi\rangle\langle\Psi|. \quad (39)$$

Given the choice of basis shown in equation (27), we can compute the following density matrix:

$$\rho_{a'b'ab} = \Psi_{a'b'} \Psi_{ba}^*. \quad (40)$$

If the Hilbert space is bipartite $\mathcal{H}^{\pi\nu} = \mathcal{H}^\pi \otimes \mathcal{H}^\nu$ then we can define the reduced density operator of a particular subspace \mathcal{H}^π to be the trace over the conjugate subspace \mathcal{H}^ν :

$$\rho^\pi = tr_\nu \rho^{\pi\nu}, \quad (41)$$

where $\rho^{\pi\nu}$ is a density operator in the space $\mathcal{H}^{\pi\nu}$ and the trace operator tr_ν contracts the indices belonging to the \mathcal{H}^ν Hilbert space. The reduced density matrix ρ^π in our choice of basis is computed from (40):

$$\begin{aligned} \rho_{a'a}^\pi &= \sum_{b'b} \delta_{b'b} (\rho_{a'b'ab}) \\ &= \sum_b \Psi_{a'b} \Psi_{ba}^* \\ &= (AA^\dagger)_{a'a}. \end{aligned} \quad (42)$$

In the SVD papers cited earlier, this density matrix was only used to compute the SVD eigenvalues. Here, we are going to take advantage of the information of mixing that is contained within the density matrix: the entanglement entropy.

The *von Neumann entropy* is defined in terms of the generalized density operator (quantum state ρ) by

$$S(\rho) \equiv -tr(\rho \ln \rho). \quad (43)$$

The *entanglement entropy* of a state in a bipartite system $\mathcal{H}^{\pi\nu} = \mathcal{H}^\pi \otimes \mathcal{H}^\nu$ is the von Neumann entropy of a reduced density matrix:

$$S(\rho^\pi) = -\text{tr}(\rho^\pi \ln \rho^\pi). \quad (44)$$

In our case, the proton-neutron entanglement entropy measures the number of quantum bits shared between the proton and neutron spaces. It is also a measure of the distribution of the SVD eigenvalues. It can be shown that $S(\rho^\pi) = S(\rho^\nu)$, from the invariance of SVD eigenvalues. We therefore simply refer to $S_{pn} \equiv S(\rho^\pi) = S(\rho^\nu)$ as the proton-neutron entanglement entropy. We first diagonalize the density matrix ρ_π and compute S_{pn} using the eigenvalues $\{\gamma_i^2\}$ of ρ_π so that

$$S_{pn} = -\sum_i \gamma_i^2 \ln(\gamma_i^2), \quad (45)$$

where γ_i are also the SVD eigenvalues of $\tilde{\Psi}_{ab}$ and Ψ_{ipjn} . The proton-neutron entanglement entropy for a given state $|\Psi\rangle$ is a measure of the entanglement of the two partitions of the Hilbert space. It indicates the degree to which an expansion

$$|\Psi\rangle = \sum_i \gamma_i |\tilde{\pi}_i\rangle |\tilde{\nu}_i\rangle \quad (46)$$

can be truncated. If the entanglement entropy is zero, then (46) contains only one term. A maximal value of S_{pn} would indicate that each term in the expansion is equally weighted; then we would have

$$S_{max} = \ln(d_p). \quad (47)$$

Let's consider a bipartite spin system $\mathcal{H}_{12} = \mathcal{H}_1 \otimes \mathcal{H}_2$ to illustrate this. We can represent any wavefunction in this space as

$$|\Psi\rangle = \sum_{ab} \Psi_{ab} |a\rangle \otimes |b\rangle \rightarrow \underline{\Psi} = \begin{bmatrix} \Psi_{\uparrow\uparrow} & \Psi_{\uparrow\downarrow} \\ \Psi_{\downarrow\uparrow} & \Psi_{\downarrow\downarrow} \end{bmatrix}, \quad (48)$$

where the basis vectors $|a\rangle$ and $|b\rangle$ are either $|\uparrow\rangle$ or $|\downarrow\rangle$, and where the elements of the matrix $\underline{\Psi}$ are the coefficients for the four possible bipartite basis states. Let's compute the entanglement entropy for two spin-1/2 particles which are not entangled:

$$|\Psi\rangle = |\uparrow\downarrow\rangle \rightarrow \underline{\Psi} = \begin{bmatrix} 0 & 1 \\ 0 & 0 \end{bmatrix}. \quad (49)$$

The reduced density matrix of this wavefunction can be computed as the matrix product $\underline{\Psi} * \underline{\Psi}^\dagger$ (see equation (42)):

$$\underline{\rho}_1 = \begin{bmatrix} 0 & 1 \\ 0 & 0 \end{bmatrix} \begin{bmatrix} 0 & 0 \\ 1 & 0 \end{bmatrix} = \begin{bmatrix} 1 & 0 \\ 0 & 0 \end{bmatrix}. \quad (50)$$

This density matrix is already diagonal, so we can compute its von Neumann entropy as

$$S_{12} = S(\rho_1) = -(1 \ln(1) + 0 \ln(0)) = 0. \quad (51)$$

Thus a non-entangled pair of spin-1/2 particles has zero entanglement entropy.

We can follow the same procedure for an entangled pair:

$$|\Psi'\rangle = \frac{1}{\sqrt{2}}(|\uparrow\downarrow\rangle - |\downarrow\uparrow\rangle), \quad (52)$$

which can be represented as a matrix using (48):

$$\underline{\Psi}' = \frac{1}{\sqrt{2}} \begin{bmatrix} 0 & 1 \\ -1 & 0 \end{bmatrix}. \quad (53)$$

The reduced density matrix is

$$\underline{\rho}' = \underline{\Psi}' * \underline{\Psi}'^\dagger = \frac{1}{2} \begin{bmatrix} 1 & 0 \\ 0 & 1 \end{bmatrix}. \quad (54)$$

Thus this entangled pair has an entanglement entropy

$$S_{12} = S(\rho_1) = -\left(\frac{1}{2} \ln\left(\frac{1}{2}\right) + \frac{1}{2} \ln\left(\frac{1}{2}\right)\right) = \ln 2, \quad (55)$$

which is the maximum entanglement entropy for a bipartite system with two-dimensional subspaces.

A lower proton-neutron entanglement entropy corresponds to a system in which we can obtain a more accurate representation of our state $|\Psi\rangle$ with fewer states in (46). The proton-neutron entanglement entropy has an advantage over the raw distribution of SVD values because we can use it to compare multiple states with a single number. In particular, if the proton-neutron entanglement entropy is smaller in nuclei where isospin is large, then we can expect such a truncation scheme to be more effective for large isospin nuclei. This is good news for the calculation of large nuclei with a large excess of neutrons. Cesium 133 has 40%

more neutrons than protons, for example. However, and this is critical, we do not yet have a criterion to find the optimal basis $\{|\tilde{\pi}_i\rangle|\tilde{\nu}_i\rangle\}$, we are only generating evidence that one exists.

We will compute the proton-neutron entanglement entropy and demonstrate that it is significantly lower for $N > Z$ nuclei than for $N = Z$ nuclei, even for nuclei with the same model space dimensions. First I will justify the use of low proton-neutron entanglement entropy as an indicator of the existence of a basis which can yield accurate truncated representations.

Particle-Hole Conjugates

The proton-neutron entanglement entropy depends on the dimension of the model space. In order for the proton-neutron entanglement entropy to be useful in comparing different nuclei, we need cases with equal or similar dimensionality. To do this, we choose to compare particle-hole conjugates.

In the interacting shell model, we reduce the effective size of the Hilbert space by redefining the vacuum state to be some inert core of nucleons, above which is a system of interacting particles. Some interacting shell model codes can also carry out “particle hole conjugation”,^{16,18} where a system of particles can be described instead by a system of holes. A hole is a gap in an otherwise filled shell. The number of valence particles is restricted to some maximum value and a filled particle state is mathematically equivalent to a hole. If a nucleus has fewer holes than particles in a model space, it is preferable to model it as a system of interacting holes. Two nuclei which are particle-hole conjugates in a model space have an equal number of proton particles and/or proton holes, and an equal number of neutron particles and/or neutron holes.

Consider the following example: ^{18}F in the sd -shell ($0d_{3/2}$, $0d_{5/2}$ and $1s_{1/2}$) has 8 inert protons and 8 inert neutrons, with one valence proton and one valence neutron, both of which are in the $0d_{3/2}$ single particle orbit. The sd -shell model space has a maximum of 12 valence particles of each type, since the space ($0d_{3/2}$, $0d_{5/2}$ and $1s_{1/2}$) has 12 unique quantum numbers in n, l, j, m . Thus ^{18}F has 12 possible states each for the proton and neutron. ^{38}K , which has 11 valence protons and 11 valence neutrons, can be represented by two particle holes in the completely filled sd -shell model space, and thus also has 12 possible states. Table 2 contains the complete set of sd -shell model space quantum numbers.

Table 6 is a collection of nuclei for which the proton-neutron entanglement entropy of the ground state were computed. Each row in the table is a particle-hole conjugate triplet, meaning every nucleus is listed in the same row as its particle-hole conjugates. For example, ^{18}F , ^{28}F , and ^{38}K are particle-hole conjugates. The numbers to the right of each nuclide are the number of valence protons (Z_{val}) and valence neutrons (N_{val}), respectively, in each nuclide's respective shell model space.

Table 6. Table of Particle-Hole Conjugate Nuclei in the sd -Shell Model Space

Inert Core	Nucleus	(Z_{val}, N_{val})		$d_p = d_n$	
^{16}O	^{18}F	(1,1)	^{28}F	(1,11)	^{38}K (11,11) 12
	^{20}Ne	(2,2)	^{28}Ne	(2,10)	^{36}Ar (10,10) 66
	^{22}Na	(3,3)	^{28}Na	(3,9)	^{34}Cl (9, 9) 220
	^{24}Mg	(4,4)	^{28}Mg	(4,8)	^{32}S (8, 8) 495
	^{26}Al	(5,5)	^{28}Al	(5,7)	^{30}P (7, 7) 792
^{40}Ca	^{42}Sc	(1,1)	^{60}Sc	(1,19)	^{78}Y (19,19) 20
	^{44}Ti	(2,2)	^{60}Ti	(2,18)	^{76}Sr (18,18) 190
	^{46}V	(3,3)	^{60}V	(3,17)	^{74}Rb (17,17) 1140
	^{48}Cr	(4,4)	^{60}Cr	(4,16)	^{72}Kr (16,16) 4845
^{56}Ni	^{58}Cu	(1,1)	^{78}Cu	(1,21)	^{98}In (21,21) 22
	^{60}Zn	(2,2)	^{78}Zn	(2,20)	^{96}Cd (20,20) 231
	^{62}Ga	(3,3)	^{78}Ga	(3,19)	^{94}Ag (19,19) 1540
	^{64}Ge	(4,4)	^{78}Ge	(4,18)	^{92}Pd (18,18) 7315
^{100}Sn	^{102}Sb	(1,1)	^{132}Sb	(1,31)	^{162}Ti (31,31) 32
	^{104}Te	(2,2)	^{132}Te	(2,30)	^{160}Hg (30,30) 496
	^{106}I	(3,3)	^{132}I	(3,29)	^{158}Au (29,29) 4960
Figure 1 symbol:	Diamond		Circle		Square

Figure 1 is a collection of proton-neutron entanglement entropies for the nuclei listed in table 6. The vertical axis is the relative proton- neutron entanglement entropy and each particle-hole conjugate triplet lies in a given column and is labeled according to its representative nucleus. Each row in table 6 is plotted in its own column. For example, the data points above ^{18}F on the horizontal axis are ^{18}F ($N = Z$), ^{28}F ($N > Z$) and ^{38}K ($N = Z$). Each of the four frames in the Figure corresponds to a different shell-model space listed in table 6.

Figure 1 demonstrates that nearly all particle-hole triplets in the four model spaces tested have the lowest proton-neutron entanglement entropy in nuclei where $N > Z$. The exceptions are the ^{18}F , ^{22}Na , and ^{26}Al triplets in the sd -shell model space and the ^{42}Sc triplet in the pf -shell model space. All four of these exceptions are odd-odd nuclei.

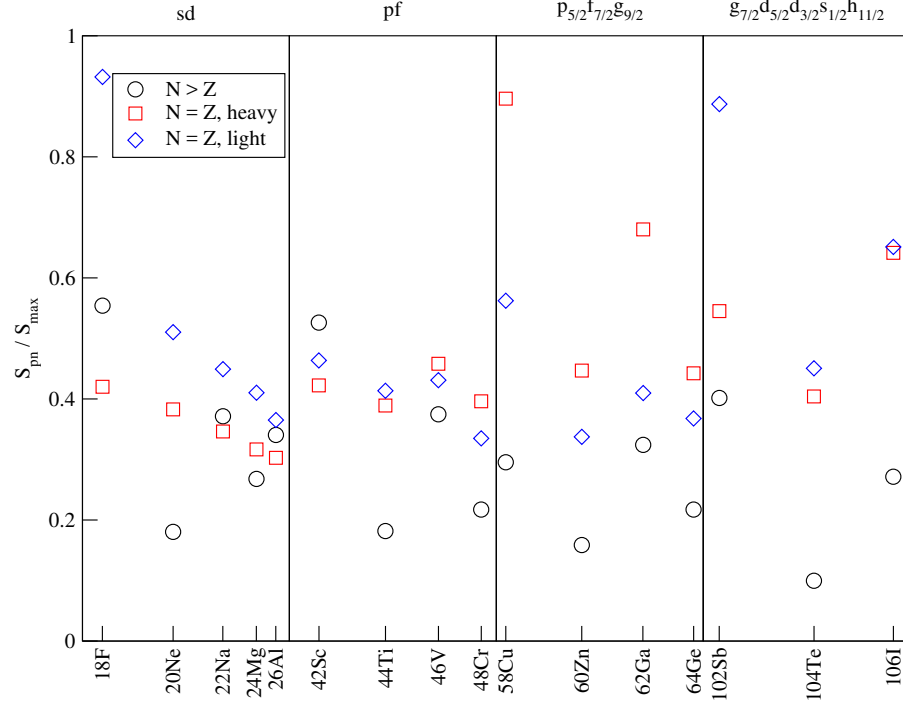


Figure 1. Normalized proton-neutron entanglement entropy for nuclei listed in Table 6. The horizontal axis labels particle-hole conjugate (PHC) triplets by the smallest nuclide in the leftmost column of Table 6 and are sorted left to right by increasing $S_{max} = \ln(\min[d_\pi, d_\nu])$. In most cases within each PHC triplet, the nuclide with an unequal numbers of protons and neutrons has the lowest entanglement entropy. All exceptions include nuclei with an odd- Z and odd- N (odd-odd) nuclide. (Circle: $N > Z$ nuclide, Square: heaviest PHC nuclide, Diamond: lightest PHC nuclide.)

Excited States and Thermalization

In order for our approach to be viable, we will need the pattern exhibited in the previous sections to hold for not just the ground state, but for excited states as well. By plotting the proton-neutron entanglement entropy for a number of the lowest energy levels, we see that $N > Z$ nuclei tend to have the lowest proton-neutron entanglement entropies only for the first few lowest eigenstates. After this, the ordering becomes apparently random. We came to the conclusion that we are observing a kind of thermalization. As the energy of the system increases, the low entropy configurations expressed in $N > Z$ nuclei disappear. An example is given in Figure 2.

Entropy and Isospin

So far we have demonstrated on a case by case basis that $N > Z$ nuclei tend to have lower proton-neutron entanglement entropy than their particle-hole conjugates. The next kind

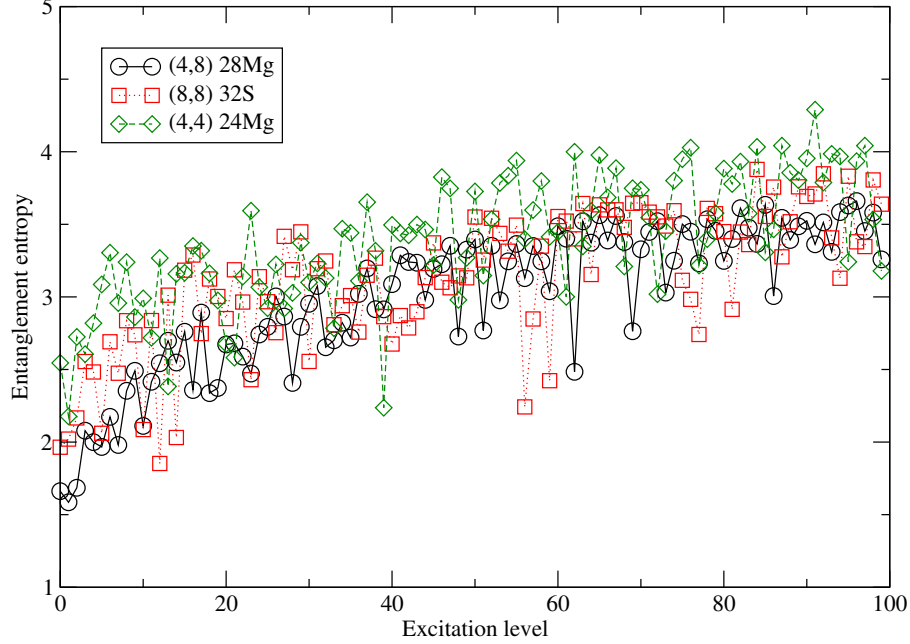


Figure 2. Proton-neutron entanglement entropy versus excitation level for ^{28}Mg and its particle-hole conjugates in the sd -shell. The entanglement entropy is lower in the ^{28}Mg spectrum for the first ten excitation levels.

of plot that we examine are plots of proton-neutron entanglement entropy S versus isospin, specifically the z -component of the isospin T_z . We will use the convention that for protons $T_z = -\frac{1}{2}$ and that for neutrons $T_z = +\frac{1}{2}$. We can then compute the maximum value of T_z for a given nucleus as $\frac{1}{2}(N - Z)$. As shown in Figures 3 as T_z increases, the proton-neutron entanglement entropy tends to decrease. This was shown in both the sd shell and the pf shell. We also extended the analysis to the sd - pf shell model space where we examined non physical nuclei with value of T_z as high as $T_z = 14$.

In Figure 3, we see that odd-odd nuclei (nuclei with odd numbers of protons and neutrons) have especially high proton-neutron entanglement. We hypothesize that this is due to the pairing interaction, which describes a tendency for pairs of nucleons to preferentially couple to $J = 0$.¹⁶ In odd-odd nuclei, one proton and one neutron are left unpaired, and it is thus thought that the pairing interaction leads to an increased interaction between these unpaired nucleons and therefore a higher proton-neutron entanglement entropy.

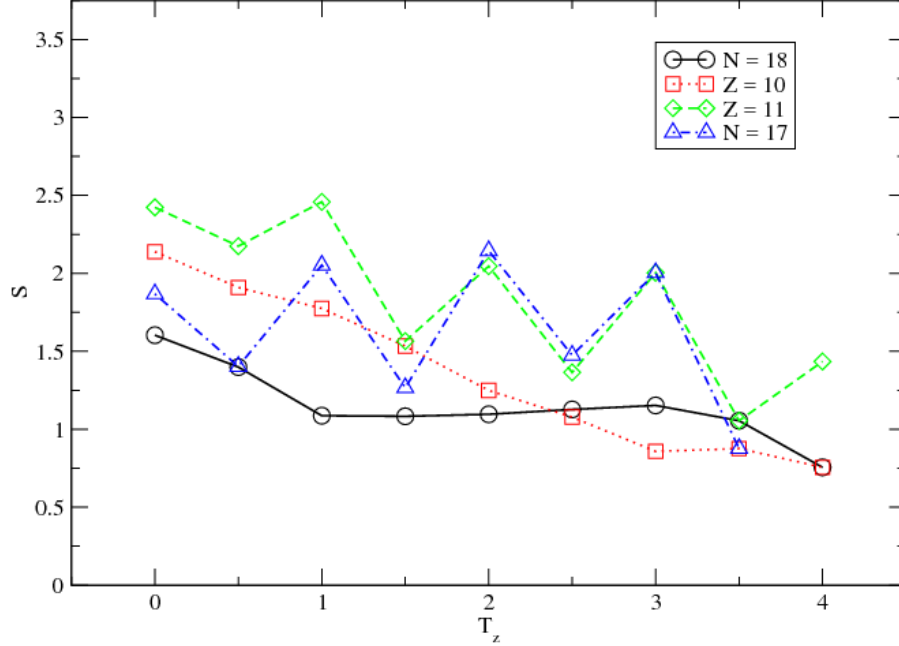


Figure 3. Entanglement entropy versus isospin for particle-hole conjugate nuclei in the *sd*-shell. Entanglement entropy tends to continuously decrease for even-even and even-odd numbers of protons and neutrons (see even-*Z* isotopes and even-*N* isotones), but to jump up for odd-odd nuclei (see odd-*Z* isotopes and odd-*N* isotones).

Dialing the Strength of the Proton-Neutron Interaction

The shell-model code BIGSTICK allows for scaling of the proton-neutron interaction term when working in the explicit proton-neutron formalism. Thus the two-body part of Hamiltonian is of the form

$$H = H_{pp} + H_{nn} + \lambda H_{pn}. \quad (56)$$

In BIGSTICK, this means scaling the two-body interaction matrix elements by λ :

$$\lambda \langle ab | V^{(pn)} | cd \rangle \quad (57)$$

We examined the relationship between the strength of the proton-neutron interaction and the relative proton-neutron entanglement entropy for the ground state of a number of nuclei. (See Figure 4.) The scaling factor λ was varied from zero, i.e. no proton-neutron interaction at all, to an order of magnitude above unity. A scaling factor of $\lambda = 1$ is a fully realistic calculation. The entanglement entropy will be zero when λ is zero because in this case there is no interaction between protons and neutrons. Essentially we have two separate and

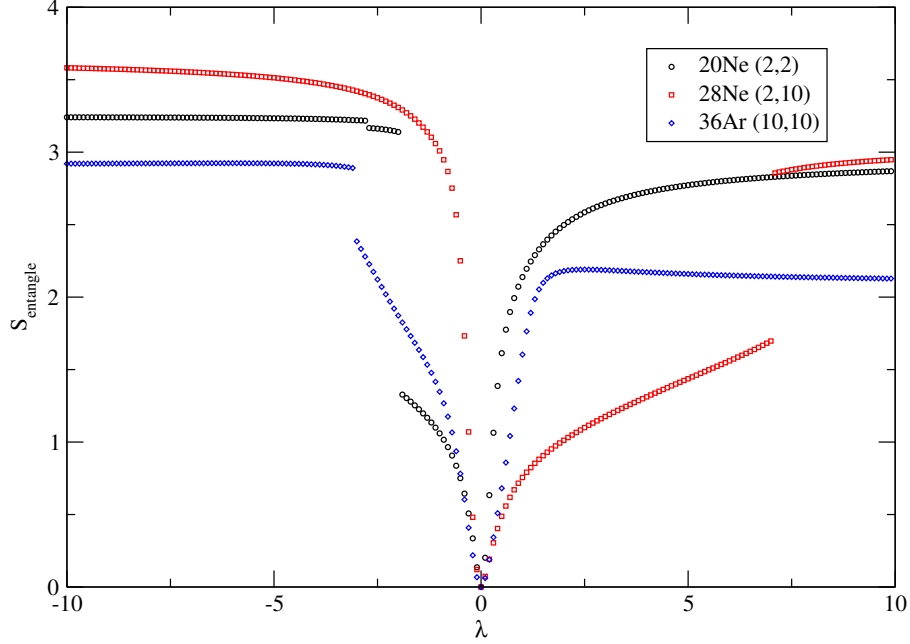


Figure 4. Proton-neutron entanglement entropy as a function of the proton-neutron two-body interaction matrix element scaling factor λ . Entanglement entropy is necessarily zero when $\lambda = 0$. $\lambda < 0$ values are non-physical but shed light on the behavior of the coupling. ^{28}Ne , with an unequal number of protons and neutrons, has the lowest entanglement entropy for values of $\lambda > 0$ up until about seven times the realistic value of $\lambda = 1$.

non-interacting model spaces. The entanglement entropy will increase as the strength of the interaction increases.

If our hypothesis that $N > Z$ nuclei converge faster in the proton-neutron formalism than $N = Z$ nuclei is correct, then we might expect different behavior in the S vs λ curves for $N > Z$ and $N = Z$ nuclei. In fact what we find is that the S vs λ curve for $N > Z$ nuclei falls below the one for $N = Z$ nuclei for nuclei of the same model space dimension. Having the same model space dimension means that the two nuclei will also have the same maximum proton-neutron entanglement entropy. This is accomplished by comparing nuclei which are particle-hole conjugates.

Figure 4 shows the dramatic difference between the S versus λ curves of nuclei with $N = Z$ versus $N > Z$. $N > Z$ have significantly lower proton-neutron entanglement entropy for values of λ greater than zero up to about five to seven times the realistic scaling of the proton-neutron interaction.

MODIFIED NUCLEAR INTERACTIONS

We have shown that proton-neutron entanglement entropy is inversely correlated with isospin; however it is not obvious why this is the case. In this section I summarize some of the attempts made to isolate the physics responsible for the behavior demonstrated in the previous chapter. To this end, I recomputed the entanglement entropy versus proton-neutron interaction strength (via the scaling factor λ) for several different nucleon-nucleon interactions.

The first series of calculations were made with *zero single particle energies*. In this interaction we start with the fully realistic nuclear interaction and then set the single particle energies equal to zero. In the many-body Hamiltonian,

$$H = \sum_{ij} \epsilon_{ij} a_i^\dagger a_i + \sum_{ijkl} a_i^\dagger a_j^\dagger V_{ijkl} a_k a_l \quad (58)$$

the single particle energies are ϵ_{ij} .

The second series of calculations were made with *traceless interactions* (see Figure 5). In this interaction we again start with the fully realistic nuclear interaction and then remove the monopole terms in the two-body interaction. These are terms of the form²⁵

$$V_{mono} = \sum_{ab} \hat{n}_a (\hat{n}_b - \delta_{ab}) U(ab), \quad (59)$$

where \hat{n} are number operators. These are related to shell structure.

The third series of calculations were made with only an attractive quadrupole-quadrupole interaction²⁶ (see Figure 6). This interaction is derived from the nuclear quadrupole moment,^{13,26}

$$Q_{ij} = \int \rho(\vec{r}) (3x_i x_j - r^2 \delta_{id}) d\vec{r}, \quad (60)$$

a tensor operator for which for microscopic expectation value for a system of nuclear matter is given by^{18,26}

$$Q_\alpha(J, M) = \langle \psi_{JM}(r_i) | \sum_i (3x_i^\alpha - r_i^2) | \psi_{JM}(r_i) \rangle, \quad (61)$$

where α is the directional orientation of the quadrupole moment of interest.

The fourth series of calculations were made with an attractive pairing interaction (see Figure 7). A problem arose when computing entanglement entropies for this interaction. The pairing interaction is known to be highly degenerate, and in cases where the eigenstates are nearly degenerate, the Lanczos method performs poorly. This is because the Lanczos method

is susceptible to loss of orthogonality of eigenstates due to numerical noise. In order to counteract this, the two-body interaction matrix elements were slightly modified. A very small random interaction was added to the matrix elements in order to desensitize the Lanczos algorithm to the degeneracies.

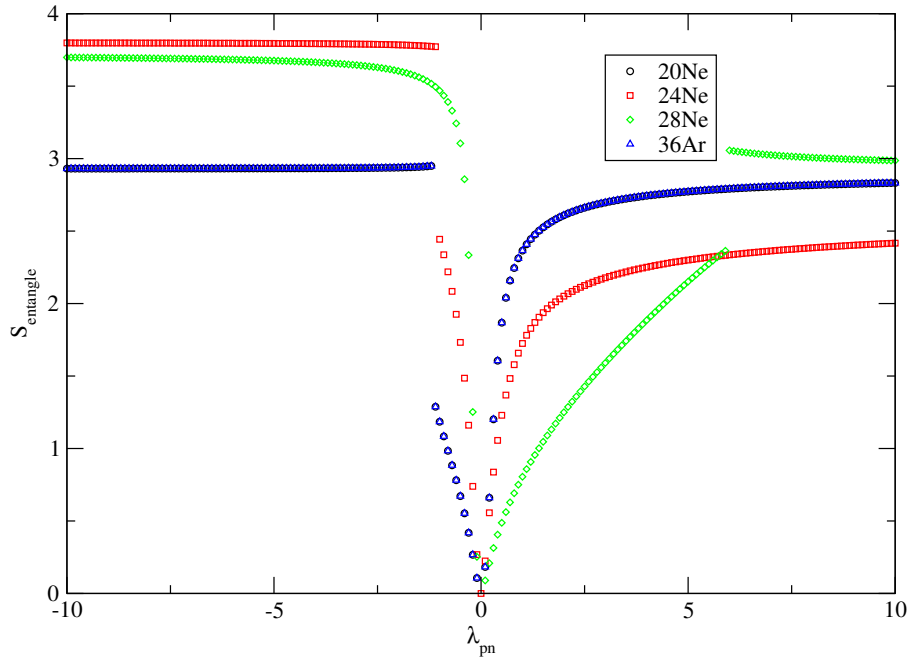


Figure 5. Entanglement entropy with a traceless interaction.

We also ran several trials with particle-hole conjugate nuclei with random two-body interactions (see Figure 8 and Figure 9). This means that all of the physics is removed and all that remains are properties of the model space. Because any given random interaction may not be particularly enlightening, we ran up to 1000 calculations with unique random interactions and plotted a histogram of the ground state entanglement entropy. In these calculations we lose the correlation between isospin and proton-neutron entanglement entropy. We often see normal distributions of the entanglement entropy for a given nucleus, and two unique modes for the distributions within a particle-hole conjugate triplet.

This study failed to reveal the source of the isospin dependence of the proton-neutron entanglement entropy. The phenomenon is not unique to any of: the pairing interaction, the quadrupole-quadrupole interaction, the full interaction with or without the monopole terms.

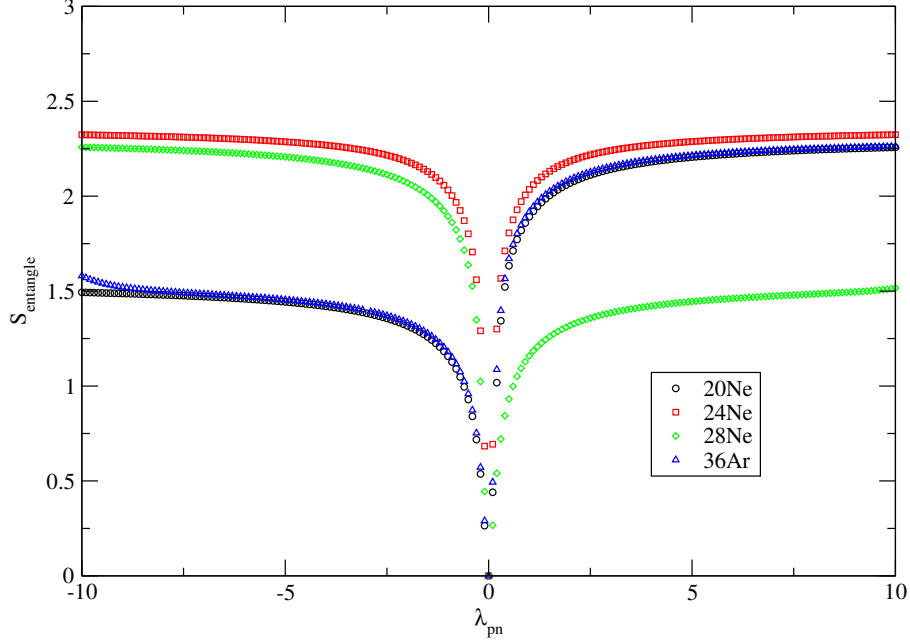


Figure 6. Entanglement entropy with an attractive quadrupole-quadrupole interaction.

TOY MODEL

I constructed a toy model to investigate the behavior of entanglement entropy of coupled systems, in an attempt to better understand the behavior seen in real nuclei such as in Figure 4. In the toy model, I consider a subspace A and a subspace B, which together form a bipartite system $\mathcal{H}_{AB} = \mathcal{H}_A \otimes \mathcal{H}_B$. \mathcal{H}_{AB} is spanned by a coupled basis:

$$|i\rangle = |a\rangle|b\rangle = |a\rangle \otimes |b\rangle, \quad (62)$$

where $|a\rangle$ are the basis states of \mathcal{H}_A and $|b\rangle$ are the basis states of \mathcal{H}_B . A Hamiltonian operator of this bipartite space could be written as

$$\hat{H} = \hat{H}_A + \hat{H}_B + \hat{H}_{AB} \quad (63)$$

where $\hat{H}_A = \hat{h}_a \otimes \hat{1}$ is an operator which acts purely in the A space, $\hat{H}_B = \hat{1} \otimes \hat{h}_b$ is an operator which acts purely in the B space and $\hat{H}_{AB} = \hat{V} \otimes \hat{W}$ is an operator which acts on both spaces. We are interested in the behavior of the system as a function of the strength of the coupling term \hat{H}_{AB} . I assume for convenience that we have already diagonalized \hat{H}_A and \hat{H}_B . I choose single particle spaces with constant energy spacing:

$$E_a \equiv \hat{h}_A|a\rangle = a\epsilon \quad (64)$$

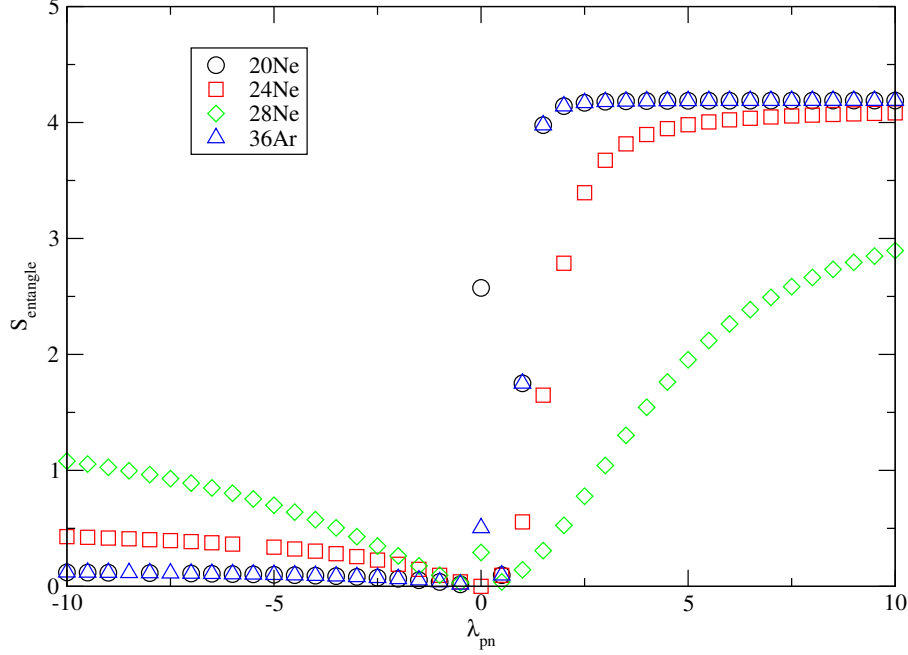


Figure 7. Attractive pairing interaction: Ne and PH-Conjugates.

for $a = 1, \dots, N$ and $\epsilon = \text{const.}$, and similarly for \hat{H}_B .

For \hat{H}_{AB} I choose an operator which is the tensor product of an operator \hat{V} in \mathcal{H}_A and an operator \hat{W} in \mathcal{H}_B . I am only interested in the behavior of the system as a function of the strength of the interaction between the subsystems, so the exact structure of each subsystem is not important. Therefore, I simply choose to fill these two matrices with a random Gaussian number generator. I symmetrically fill an $N \times N$ matrix with random numbers centered at zero with a standard deviation of 2σ for the diagonal matrix elements, and σ for the off-diagonal matrix, a standard practice for generating real, symmetric random matrices. Finally, I include a two-body matrix elements (TBME) scaling factor λ :

$$\hat{H}_{AB} = \lambda \hat{V} \otimes \hat{W} \quad (65)$$

It is now straightforward to calculate the matrix elements of the Hamiltonian. As above, let a, a' label the proton states and b, b' label the neutron states. These run from 1 to N . Now let $i = a + N(b - 1)$ label the many-body state, which runs from 1 to N^2 . Then

$$\langle i' | \hat{H} | i \rangle = H_{i',i} = \delta_{a'a} \delta_{b'b} (E_a + E_b) + \lambda V_{a'a} W_{b'b}. \quad (66)$$

$V_{a'a}$ and $W_{b'b}$ are real, symmetric, $N \times N$ random matrices with Gaussian distributions:

$$P(V_{aa'}) \sim \exp\left(-\frac{V_{aa'}^2}{2\sigma^2(1 + \delta_{a'a})}\right), \quad (67)$$

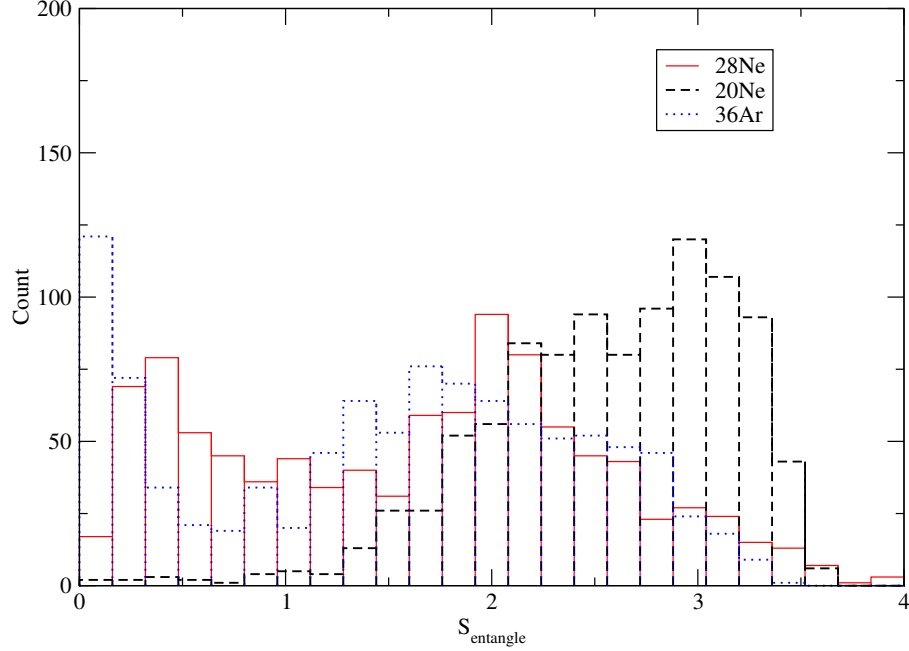


Figure 8. Random interactions exhibiting a bimodal distribution of entanglement entropy. No apparent correlation between entanglement entropy and ratio of protons to neutrons.

a Gaussian distribution of σ for the off-diagonals and 2σ for the diagonals.

Once we diagonalize the model Hamiltonian, we want to quantify how the entanglement entropy is affected by the coupling- term scaling factor λ and by the two interactions are the same $W = V$ or different $W \neq V$. This is meant to model the behavior of the nuclear Hamiltonian when and its distinct S_{pn} versus λ curves for when the number of protons is the same or different from the number of neutrons.

Suppose that we diagonalize the Hamiltonian and that

$$\hat{H}|\psi\rangle_i = E_i|\psi\rangle_i \quad (68)$$

defines our N^2 eigenstates. Any given state can be written as

$$|\psi\rangle = \sum_i c_i |i\rangle = \sum_{a,b} c_{ab} |a\rangle |b\rangle, \quad (69)$$

and so the reduced density matrix ρ_A of $|\Psi\rangle$ is the partial trace,

$$\rho_A = \text{tr}_b \rho. \quad (70)$$

Given our choice of indexing, this is computed as

$$\rho_p(a', a) = \sum_{b=1}^N c_{a'b} c_{ab}^*. \quad (71)$$

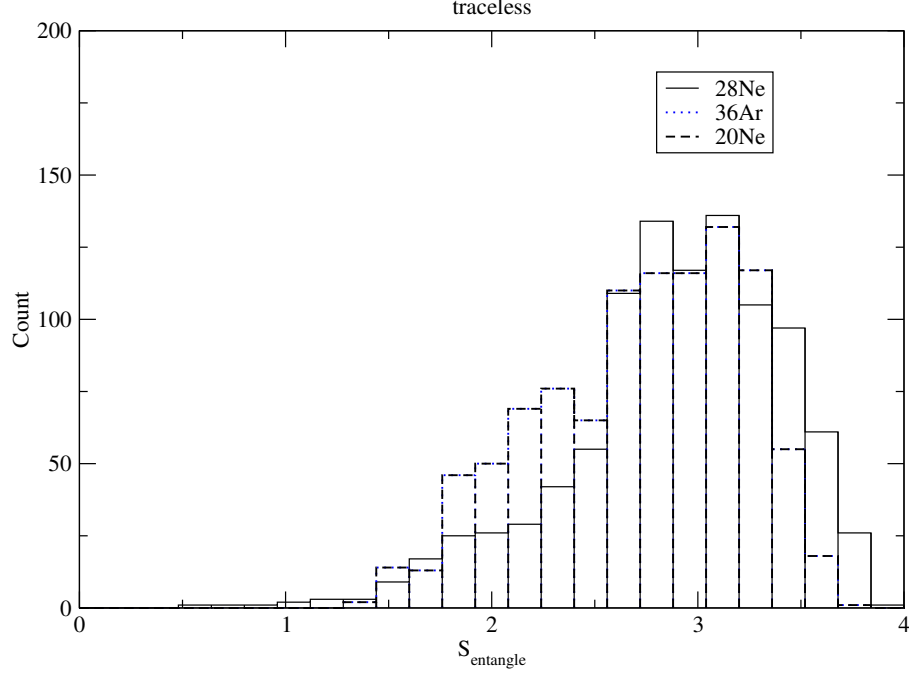


Figure 9. Random traceless interactions exhibiting a unimodal distribution of entanglement entropy. No apparent correlation between entanglement entropy and ration of protons to neutrons. $N = Z$ nuclei have the same entanglement entropy for all interactions, as expected.

We can now define the proton-neutron entanglement entropy of the state described by ρ to be the *von Neumann* entropy of the reduced density matrix ρ_p ,

$$S_{pn} = -\text{tr} \rho_p \ln \rho_p. \quad (72)$$

If we first diagonalize ρ_p to find its N eigenvalues γ_i^2 then the entanglement entropy becomes

$$S_{pn} = -\sum_{i=1}^N \gamma_i^2 \ln \gamma_i^2. \quad (73)$$

This quantity measures the entanglement entropy, or the mixing of quantum bits, of the two subspaces in a given state of the Hamiltonian.

In the first adaption of this toy model we has Hamiltonian matrix elements exactly as they appear in equation (66). Here, $\epsilon = 1$, $\sigma = 1$, and two curves are plotted: one in which the random matrices V and W are the same and one in which they are different. In these models we saw that when the two interactions W and V are the same, the entanglement entropy tends towards some finite non-zero value, whereas when W and V are different, the entanglement entropy falls off to zero. This tells us that the entanglement entropy can differ between two

systems of the same dimension depending on the similarity of the interactions acting between the subspaces. Mathematically this has to do with the orthogonality of the eigenstates of the interactions within each subspace. In another adaption of the model, we start with two identical subspaces and then slowly change one of the subspaces to be different from the original.

$$H = E^V + E^W + \lambda(V \otimes (V + \delta W)) \quad (74)$$

In doing so we can see in Figure 10 that as the two interactions diverge, the entanglement entropy of the system falls off from its maximum convergent value. When the perturbative parameter $\delta = 0$, equation (74) reduces to equation (66) for the case when $W = V$.

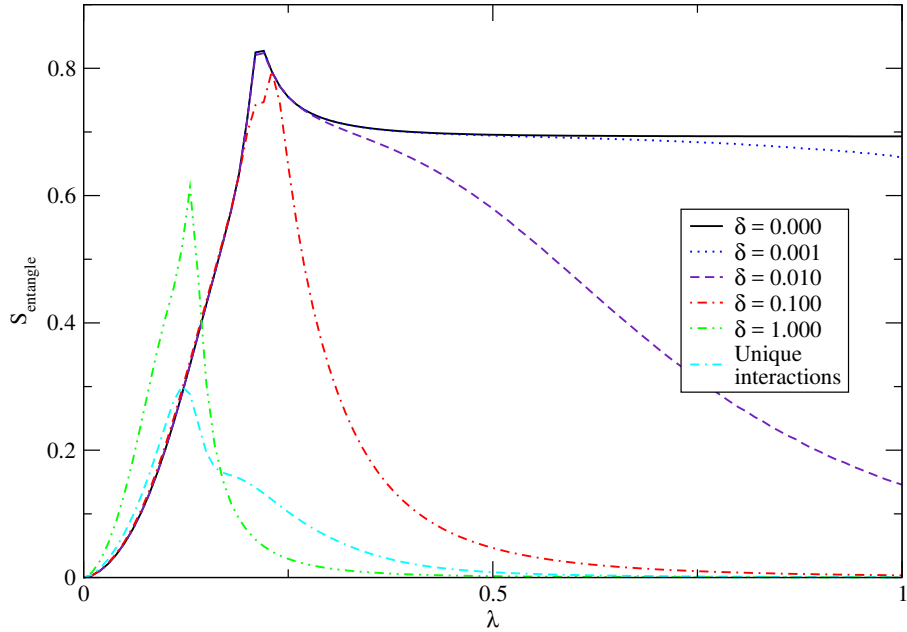


Figure 10. Toy Model with perturbative variance of the interaction W away from V . The subspaces containing the V interaction has the same dimensions as the subspace containing the W interaction. See equation (74).

In an attempt to get convergence to non-zero entanglement entropies when $W \neq V$, which is what we see in the nuclear calculations, I suggested the following Hamiltonian on the grounds that a constant term may prevent the entanglement entropy from converging to zero when the two species of interactions are different:

$$H_{i',i} = \delta_{a'a} \delta_{b'b} (E_a + E_b) + \lambda (V_{a'a} W_{b'b} + V_{a'a} + W_{b'b}), \quad (75)$$

which implicitly is a Hamiltonian of the form

$$H = E^V + E^W + \lambda(V \otimes W + V \otimes I + I \otimes W), \quad (76)$$

where E is diagonal. By using an explicitly non-separable interaction, we obtained the desirable feature than $W \neq V$ curves converged to non-zero entanglement entropy. However, curves generated with different random number generator seeds produced varying results, some exhibiting anomalous spikes in entropy near the origin.

The next most obvious adaption was to simply include a several terms in the coupling part of the Hamiltonian:

$$H_{i',i} = \delta_{a'a} \delta_{b'b} (E_a + E_b) + \lambda \left(\sum_i V_{a'a}^i W_{b'b}^i \right), \quad (77)$$

which is a Hamiltonian of the form:

$$H = E^{(V)} + E^{(W)} + \lambda \left(\sum_i V_i \otimes W_i \right), \quad (78)$$

where each The results of this toy model are shown in Figure 11. This version of the toy model has the following features:

- Entanglement entropy goes to zero at the origin
- Dependence on the random number generator seed goes down with the number of terms in the sum
- Entanglement entropy convergences to nonzero entanglement entropies at large λ for different subspaces, and
- Very few anomalous features, such as spikes in entanglement entropy

However, the model still doesn't have the same features as the realistic proton-neutron entanglement entropy, namely, symmetric entanglement entropy curves when the both species' interactions are identical, and, when the interactions are different: lower entanglement entropy for positive λ and higher entanglement entropy for negative λ . See Figure 11 (a) and (b) for comparison. Several dozen other toy model Hamiltonians were investigated, including those with different single species interactions, and models with different dimensions. However, I failed to find a model which reliably produces S versus λ curves with the same topology as in the nuclear Hamiltonian.

SUMMARY ON ENTANGLEMENT ENTROPY

We investigated the properties of the proton-neutron entanglement entropy, which is an indicator used to determine whether or not certain wavefunctions could be represented more efficiently in some basis. We showed that nuclei with unequal numbers of protons and neutrons have a lower entanglement entropy, which means that $N > Z$ nuclei may have even more efficient representations. We attempted to understand the properties of the entanglement entropy, but more investigation is needed. The toy model we investigated tells us that the phenomenon of higher entanglement entropy in systems with identical subspaces is more ubiquitous than the nuclear many-body problem. Moving on from this section, readers should keep in mind that we have evidence for the existence of efficient representations of our nuclear wavefunctions, but have yet to inquire about which basis will yield these efficient representations. This will be addressed in the next chapter.

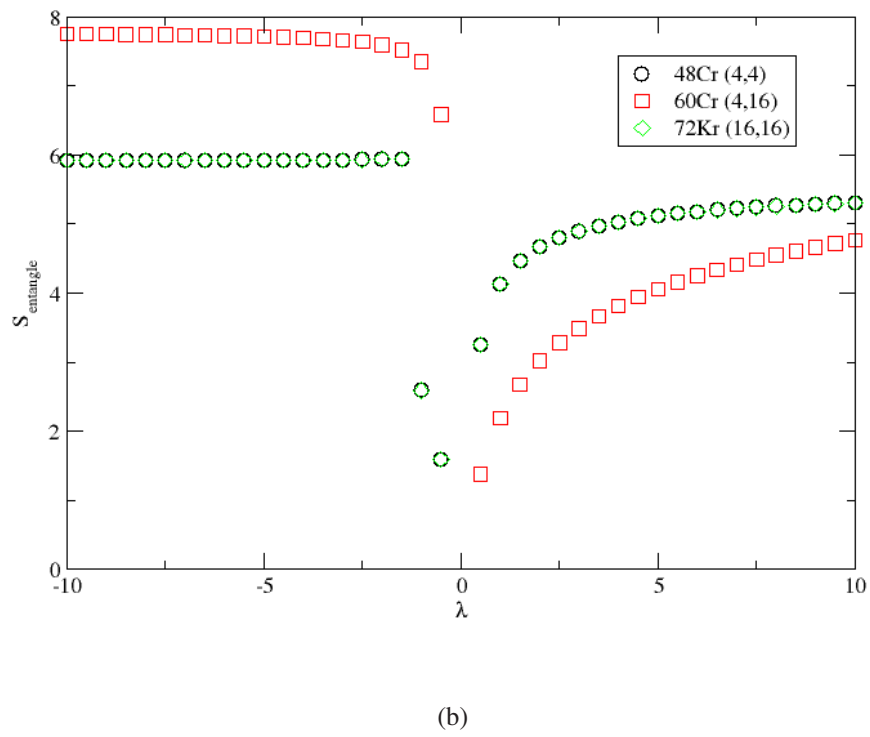
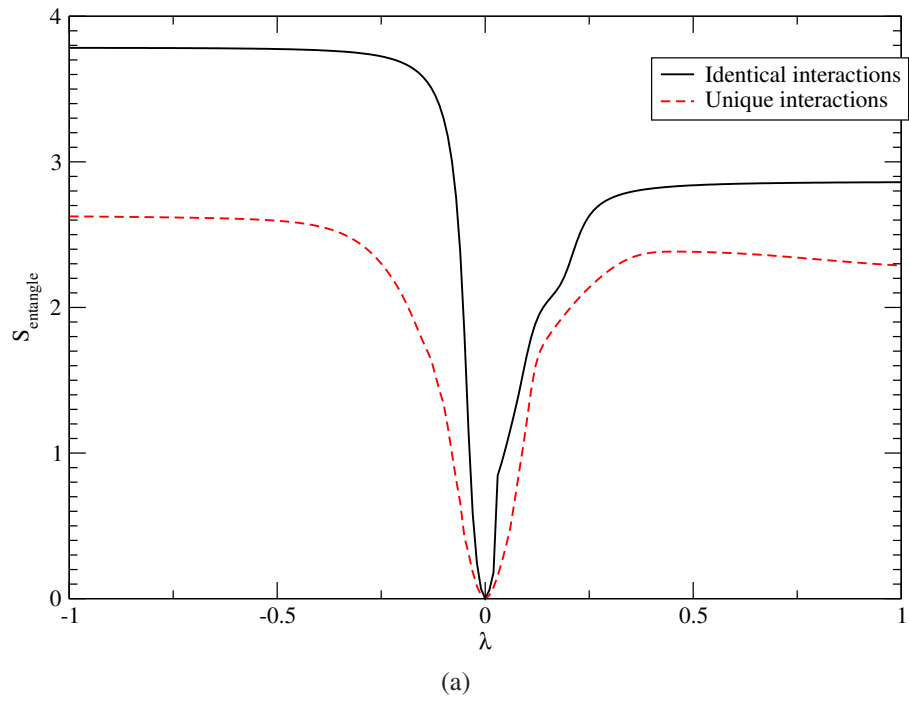


Figure 11. Entanglement entropy S versus scaling factor λ for (a) toy model with non-separable two-body terms, and (b) nuclei in the pf -shell with a traceless interaction.

CHAPTER 4

PROTON-NEUTRON DECOMPOSITION

In the previous chapter, we studied the distribution of wavefunction coefficients in order to provide evidence that there exists a basis in which our nuclear wavefunctions could be truncated, thus allowing more efficient representation of the wavefunctions. Ultimately our goal is to find a basis in which our Hamiltonian can be truncated. In this chapter I will examine a decomposition of wavefunctions which corresponds to a particular framework for computing truncated Hamiltonian matrix elements.

We will be assuming that our Hamiltonian can be decomposed as

$$\hat{H} = \hat{H}_{proton} + \hat{H}_{neutron} + \hat{H}_{proton-neutron} \quad (79)$$

where \hat{H}_{proton} contains all interactions between protons, $\hat{H}_{neutron}$ contains all interactions between neutrons, and $\hat{H}_{proton-neutron}$ contains all remaining interactions between protons and neutrons. Then we call the eigenstates of the pure-proton Hamiltonian $|\pi\rangle$, as in

$$H_{proton}|\pi\rangle = E_p|\pi\rangle, \quad (80)$$

and the eigenstates of the pure-neutron Hamiltonian are equivalently define for $\hat{H}_{neutron}$ and $|\nu\rangle$. Roughly speaking, our proposed truncation scheme is to compute the full Hamiltonian (79) in a basis built up from the coupled eigenstates of \hat{H}_{proton} and $\hat{H}_{neutron}$. It was therefore worth decomposing existing wavefunctions $|\Psi\rangle$ into the eigenstates of both pure-proton interaction operators and pure-neutron interaction operators. This will tell us how whether or not truncating a basis of coupled pure-proton and pure-neutron wavefunctions will be viable. To see why, consider an arbitrary wavefunction $|\Psi\rangle$. To expand $|\Psi\rangle$ into a basis $\{|\alpha\rangle\}$, one first computes the coefficients

$$c_\alpha = \langle\alpha|\Psi\rangle. \quad (81)$$

If some significant subset of the coefficients $\{|\alpha\rangle\}$ are much smaller than the rest, then the full wavefunction,

$$|\Psi\rangle = \sum_{\alpha} c_{\alpha} |\alpha\rangle, \quad (82)$$

could be represented by just a few terms. What we care about is the magnitude of the coefficients $\{|\alpha\rangle\}$, thus we could instead compute

$$|c_\alpha|^2 = \langle \Psi | \alpha \rangle \langle \alpha | \Psi \rangle, \quad (83)$$

where the object $|\alpha\rangle\langle\alpha|$ is a projection operator.

We computed the equivalent set of coefficients (83) for our nuclear wavefunctions projected onto the eigenstates of \hat{H}_{proton} and $\hat{H}_{neutron}$. This was done using existing capabilities in BIGSTICK to compute transition strength functions. In particular I used the option to decompose wavefunctions onto scalar operators.¹⁵ To do this, we first solve for the wavefunction $|\Psi\rangle$ for some nucleus. Then BIGSTICK solves equation (80) and the equivalent equation for the neutron Hamiltonian, using its Lanczos capabilities to find low-lying eigenstates $|\pi_a\rangle$ (or $|\nu_a\rangle$). Then, the nuclear wavefunction is projected onto these eigenstates in the following manner:

$$\begin{aligned} \langle \pi_a | \Psi \rangle &= \langle \pi_a | \sum_{a,b} \tilde{\Psi}_{ab} | \pi_a \rangle | \nu_b \rangle \\ &= \sum_b \tilde{\Psi}_{ab} | \nu_b \rangle. \end{aligned} \quad (84)$$

The strengths of these projections is then computed as

$$\begin{aligned} \langle \Psi | \pi'_a \rangle \langle \pi_a | \Psi \rangle &= \sum_b \tilde{\Psi}_{a'b}^* \tilde{\Psi}_{ab} \\ &= \sum_b^{N_{keep}} |\Psi_{ab}|^2 \\ &\equiv c_a^2. \end{aligned} \quad (85)$$

The quantities c_a^2 are the strengths of the projection of a wavefunction $|\Psi\rangle$ onto the proton-proton interaction eigenstate $|\pi_a\rangle$. Since we are assuming a set of normalized wavefunctions in our basis,

$$1 = \sum_a \langle \pi_a | \pi_a \rangle, \quad (86)$$

and thus the strengths c_a^2 are the fractions of the total wavefunction $|\Psi\rangle$ contained in the state $|\pi_a\rangle$.

I projected nuclear wavefunctions onto the eigenstates of the proton Hamiltonian of the neutron Hamiltonian and plotted the strengths c_X^2 for each interaction as a function of the

eigenstate number. A typical set of results is shown in Figure 12 and Figure 13. The vertical axis is the strength of the decomposition onto the eigenstate of either the proton Hamiltonian or the neutron Hamiltonian with the X^{th} lowest energy. Each plot has two sets of values, one for each of two particle-hole conjugate nuclei in the sd -shell: one being the proton (PP) decomposition and the other being the neutron (NN) decomposition.

There are two important conclusions to be drawn from these decompositions. The first is that the strengths fall off rapidly in the first handful of states. This suggests that a truncation of the coupled pure-proton and pure-neutron eigenstates could be a viable method for obtaining approximate wavefunctions. However it is already known that this is the case for light nuclei.^{21–23} The second important feature is apparent when plotting the strength function decompositions for particle-hole conjugate nuclei on the same plot. We find that even though these pairs of nuclei have the same dimensions in their shell model spaces, nuclei for which $N > Z$ have strengths which are significantly lower than their $N = Z$ conjugates. This is further evidence that the same proposed truncation scheme may be even more effective in heavier nu

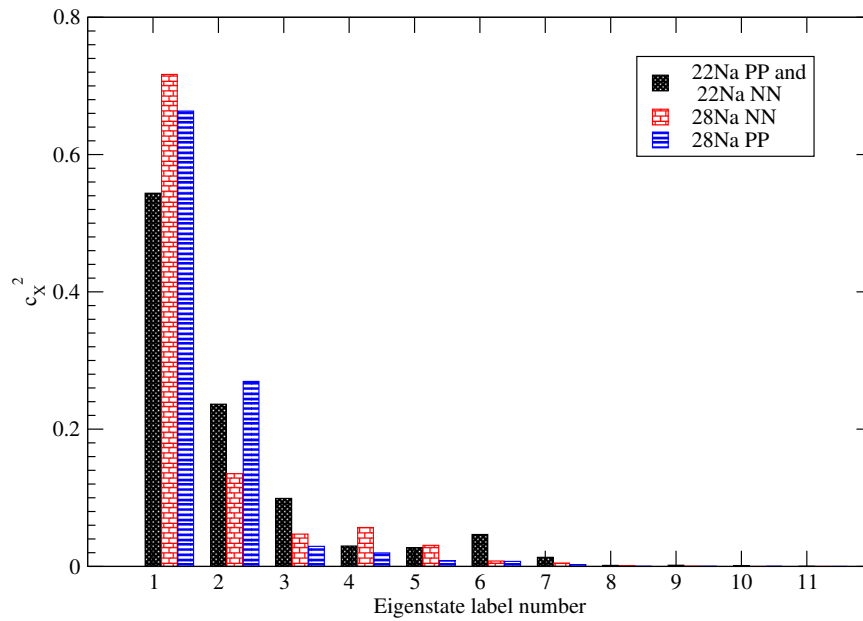


Figure 12. Strength decomposition of nuclear wavefunctions into eigenstates of the proton-proton or neutron-neutron interaction for two particle-hole conjugate nuclei in the sd -shell. Strengths fall off exponentially.

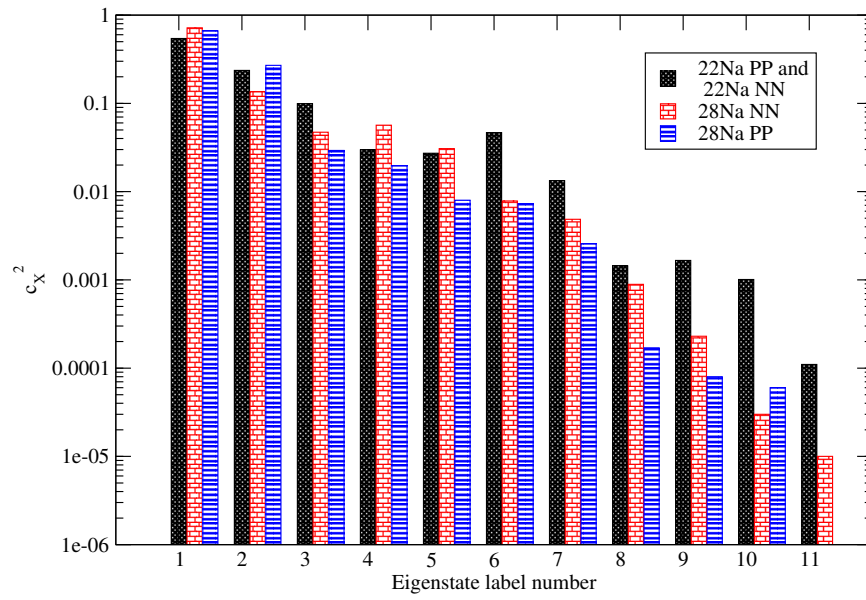


Figure 13. Strength decomposition of nuclear wavefunctions into eigenstates of the proton-proton or neutron-neutron interaction for two particle-hole conjugate nuclei in the sd -shell. The decomposition strengths of ^{28}Na , with an unequal number of protons and neutrons, fall off faster than its conjugate, suggesting that fewer states are necessary to represent it.

CHAPTER 5

PNISM

Finally, we turn to the main subject of this thesis, our Proton-Neutron Interacting Shell Model (PNISM) code. We are motivated by the results of the previous chapters; it is known that SVD eigenvalues of wavefunction coefficients fall off exponentially, and we have seen that they fall off even faster in nuclei with unequal numbers of protons and neutrons. We also argued that the basis states formed from the eigenstates of the proton interaction and the neutron interaction could likely allow for truncated wavefunctions. We have reason to believe that truncation of the model space in a weakly coupled proton-neutron basis might be an especially effective approximation for heavier nuclei with more neutrons than protons. We set out to write a code that couples together eigenstates of the proton Hamiltonian and eigenstates of the neutron Hamiltonian to create a many-proton many-neutron basis. The matrix elements of the full Hamiltonian are then computed in this basis, which is truncated.

This chapter will derive the equations used to carry out the calculation of the Hamiltonian matrix elements from the eigenstates computed by the interacting shell model code BIGSTICK. Calculation of the one-body density matrices of the resulting wavefunctions is also discussed. The following chapter will discuss the details of the code itself.

THE HAMILTONIAN

We write the nuclear Hamiltonian in explicit proton-neutron formalism. The Hamiltonian operator in the second quantization formalism,

$$\hat{H} = \sum_{ab} \langle a|T|b \rangle \hat{c}_a^\dagger \hat{c}_b + \frac{1}{4} \sum_{abcd} \langle ab|V|cd \rangle \hat{c}_a^\dagger \hat{c}_b^\dagger \hat{c}_c \hat{c}_d, \quad (87)$$

can be written as a sum of terms separated by nucleon species:⁸

$$\hat{H} = \hat{H}_p + \hat{H}_n + \hat{H}_{pp} + \hat{H}_{nn} + \hat{H}_{pn}, \quad (88)$$

where \hat{H}_p and \hat{H}_{pp} are one- and two-body Hamiltonians, respectively, which act only on protons, \hat{H}_n and \hat{H}_{nn} act only on neutrons, and \hat{H}_{pn} contains the remaining interactions

between proton and neutrons. To this end, it is useful to define the two body creation operator:²⁶

$$\hat{A}_{JM}^\dagger(ab) \equiv [c_a^\dagger \otimes c_b^\dagger]_{JM} \quad (89)$$

Here, the total angular momentum J and the azimuthal or magnetic quantum number $M = J_z$ are needed for the coupling of the two one-body creation operators, via Clebsch-Gordan coefficients:²⁷

$$[c_a^\dagger \otimes c_b^\dagger]_{JM} = \sum_{m_a m_b} (j_a m_a, j_b m_b | JM) \hat{c}_{j_a m_a}^\dagger \hat{c}_{j_b m_b}^\dagger. \quad (90)$$

The two-body creation and annihilation operators²⁸ with fixed J and M are thus, respectively:

$$\begin{aligned} A_{JM}^\dagger &= \sum_{m_a m_b} (j_a m_a, j_b m_b | JM) c_{j_a m_a}^\dagger c_{j_b m_b}^\dagger, \text{ and} \\ A_{JM} &= \sum_{m_c m_d} (j_c m_c, j_d m_d | JM) c_{j_c m_c} c_{j_d m_d}. \end{aligned} \quad (91)$$

These will be used later in the derivation of the proton-neutron interaction matrix elements.

With these definitions, two-body states with proper normalization are¹⁶

$$|ab; JM\rangle \equiv \frac{1}{\sqrt{1 + \delta_{ab}}} \hat{A}_{JM}^\dagger(ab) |0\rangle. \quad (92)$$

The two-body part of the Hamiltonian is thus expressed

$$\begin{aligned} \hat{H}_{2b} &= \sum_{abcd} c_a^\dagger c_b^\dagger \langle ab | V | cd \rangle \hat{c}_c \hat{c}_d \\ &= \frac{1}{4} \sum_{abcd} \zeta_{ab} \zeta_{cd} \sum_J \langle ab; JM | V | cd; JM \rangle \sum_M A_{JM}^\dagger(ab) A_{JM}(cd) \end{aligned} \quad (93)$$

where $\zeta_{ab} \equiv \sqrt{(1 + \delta_{ab})}$. Our next move is to change to an explicit proton-neutron decomposition. This can be done by using the states $\frac{1}{\sqrt{2}}(|\pi\nu\rangle - |\nu\pi\rangle)$, $\frac{1}{2}(|\pi\nu\rangle + |\nu\pi\rangle)$, $|\pi\pi\rangle$, and $|\nu\nu\rangle$ to isolate operators by the nucleon species on which they act. The result is the following proton-proton two-body interaction:

$$\hat{H}_{pp} = \frac{1}{4} \sum_{abcd} \zeta_{ab} \zeta_{cd} \sum_J V_J^{pp}(ab, cd) \sum_M \hat{A}_{JM}^\dagger(a_\pi b_\pi) \hat{A}_{JM}(c_\pi d_\pi). \quad (94)$$

\hat{H}_{nn} has the same form. We will not use these directly but it is useful to see how the interaction is separated. The proton-neutron interaction is the only term that will be used directly in our code:

$$H_{pn} = \sum_{abcd} \sum_J V_J^{(pn)}(ab, cd) \sum_M A_{JM}^\dagger(a_\pi b_\nu) A_{JM}(c_\pi d_\nu). \quad (95)$$

THE BASIS

We have a Hamiltonian of the form (88) and in order to compute its matrix elements, we need to choose a basis, one which we hope we can truncate effectively. In this section I will explain our choice of basis and how we select which states to truncate. In the future we will want to develop a more sophisticated approximation scheme to improve our results. For now we first solve

$$\begin{aligned}(\hat{H}_p + \hat{H}_{pp})|\Psi_p\rangle &= E_p|\Psi_p\rangle \text{ and} \\(\hat{H}_n + H_{nn})|\Psi_n\rangle &= E_n|\Psi_n\rangle,\end{aligned}\tag{96}$$

and set our uncoupled basis states equal to the solutions:

$$\begin{aligned}|J_p^{\pi_p}, \alpha_p\rangle &= |\Psi_p\rangle, \\|J_n^{\pi_n}, \beta_n\rangle &= |\Psi_n\rangle,\end{aligned}\tag{97}$$

where J_p is the total angular momentum of the proton state, π_p is its parity, and α_p is just a state label, and equivalently for the neutron states. We build our many-body basis states by coupling together these proton and neutron states:

$$|J_p^{\pi_p}, \alpha_p\rangle \otimes |J_n^{\pi_n}, \beta_n\rangle.\tag{98}$$

Our solutions to (96) yield d_π pure proton eigenstates and d_π pure neutron eigenstates. The eigenstates of a Hermitian operator form a complete set of orthogonal eigenvectors. Assuming these are normalized, any many-body wavefunction can be expanded:

$$|\Psi\rangle = \sum_{\alpha_p}^{d_\pi} \sum_{\beta_n}^{d_\pi} \Psi_{\alpha_p\beta_n} |J_p^{\pi_p}, \alpha_p\rangle \otimes |J_n^{\pi_n}, \beta_n\rangle.\tag{99}$$

Therefore these states can be used to compute the matrix elements of the full Hamiltonian (88), where $\hat{H}_p + \hat{H}_{pp}$ and $\hat{H}_n + H_{nn}$ are now used in their diagonal forms.

So far all we have done is to solve the nuclear Hamiltonian in a basis of coupled proton and neutron states by solving the proton and neutron interactions separately. The computational advantage to this procedure lies in the prospect of truncating the model space. In doing so, we will have to make choices to ensure that the eigenstates of the truncated Hamiltonian remain eigenstates of J^2 . If we were to truncate the basis in an M-Scheme procedure, then our solutions would not be guaranteed to have good total angular momentum. To see why, consider the following example for a two state system. Imagine a basis with two

states $\frac{1}{\sqrt{2}}(|z; +\rangle + |z; -\rangle)$ and $\frac{1}{\sqrt{2}}(|z; +\rangle - |z; -\rangle)$. If we were truncate to just one of either of these states, then any solution in the truncated basis could not be an eigenstate of \hat{S}_z .

Similarly, a truncated M-scheme basis is not guaranteed to have good total angular momentum. Therefore, we choose a basis with good total angular momentum so that even once we truncate the basis we are guaranteed to get solutions with good total angular momentum. This is called a J-scheme.

Therefore we choose to couple our proton and neutron states in such a way as to be eigenstates of \hat{J}^2 :

$$[|J_p^{\pi_p}, \alpha_p\rangle \otimes |J_n^{\pi_n}, \beta_n\rangle]_{J^\pi} \equiv |J_p^{\pi_p}, \alpha_p, J_n^{\pi_n}, \beta_n; J^\pi\rangle, \quad (100)$$

A wavefunction expanded in this basis is of the form

$$|\Psi\rangle = \sum_{\alpha_p \beta_n}^Q \Psi_{\alpha_p \beta_n} |J_p^{\pi_p}, \alpha_p, J_n^{\pi_n}, \beta_n; J^\pi\rangle, \quad (101)$$

and is guaranteed to have good total J . Here, the sum runs up to Q , which will be chosen to be $Q \ll \min[d_p, d_n]$ when computing the matrix elements of (88).

FACTORIZING THE PROTON-NEUTRON INTERACTION

To calculate the matrix elements of H_{pn} , we refactor equation (95) into one-body density-like operators whose matrix elements can be computed from the density matrices found from solving the single-species terms (see equation (96)) of the full Hamiltonian (88). Equation (95) is written as a product of pair creation and annihilation operators. These can be reordered into one-body density operators. Doing so will introduce a nontrivial phase and a number of identities involving vector coupling coefficients will be applied.

Expanding equation (95) using (91), we obtain

$$H_{pn} = \sum_{abcd} \sum_J V_J^{(pn)}(ab, cd) \sum_M \sum_{m_a m_b} \sum_{m_c m_d} (j_a m_a, j_b m_b | JM) (j_c m_c, j_d m_d | JM) c_{j_a m_a}^\dagger c_{j_b m_b}^\dagger c_{j_c m_c} c_{j_d m_d}, \quad (102)$$

where the sums are constrained such that $M = m_a + m_b = m_c + m_d$. We want to write (102) in terms of the the generalized one-body density operator:²⁶

$$\rho_{K\mu}(a\tilde{c}) \equiv \sum_{m_a m_c} (j_a m_a, j_c - m_c | K\mu) c_{j_a m_a}^\dagger \tilde{c}_{j_c - m_c}. \quad (103)$$

Given the definition of a time-reversed annihilation operator,²⁷

$$\tilde{c}_{j_c - m_c} = (-1)^{j_c - m_c} c_{j_c m_c}, \quad (104)$$

we write the generalized one-body density operator in terms of the same creation/annihilation operators that appear in (102):

$$\rho_{K\mu}(a\tilde{c}) = \sum_{m_a m_c} (j_a m_a, j_c - m_c | K\mu) (-1)^{j_c - m_c} c_{j_a m_a}^\dagger c_{j_c m_c}. \quad (105)$$

The tilde over the index c reminds us the time reversal operator was used. To move further we need to recouple the vector coupling coefficients in (102) to match the coefficients in the definition (105). This requires *six-J symbols*,²⁷ an invariant generalization of vector coupling coefficients. A brief introduction to vector coupling coefficients and six-J symbols are given in Appendix A. We will need the following relationship between vector-coupling coefficients and the six-J symbol:²⁷

$$\begin{aligned} (j_a m_a, j_b m_b | JM) (j_c m_c, j_d m_d | JM) = \\ \sum_{K\mu} (-1)^{J+M} (-1)^{j_b - j_d + \mu} (2J + 1) \begin{Bmatrix} j_a & j_b & J \\ j_d & j_c & K \end{Bmatrix} \\ (j_a m_a, j_c - m_c | K\mu) (j_b m_b, j_d - m_d | K - \mu). \end{aligned} \quad (106)$$

Now that we have what we need, we start again with (95) and sequentially apply these definitions and identities. The pair creation and annihilation operators in (95) can be rewritten using (106):

$$\begin{aligned} \sum_M A_{JM}^\dagger(ab) A_{JM}(cd) \\ = \sum_M \sum_{m_a m_b} \sum_{m_c m_d} (j_a m_a, j_b m_b | JM) (j_c m_c, j_d m_d | JM) c_{j_a m_a}^\dagger c_{j_b m_b}^\dagger c_{j_c m_c} c_{j_d m_d} \\ = \sum_M \sum_{m_a m_b} \sum_{m_c m_d} \sum_{K\mu} (-1)^{J+M} (-1)^{j_b - j_d + \mu} (2J + 1) \begin{Bmatrix} j_a & j_b & J \\ j_d & j_c & K \end{Bmatrix} \\ (j_a m_a, j_c - m_c | K\mu) (j_b m_b, j_d - m_d | K - \mu) c_{j_a m_a}^\dagger c_{j_b m_b}^\dagger c_{j_c m_c} c_{j_d m_d} \end{aligned} \quad (107)$$

We apply an anticommutation relation to reorder the creation/annihilation operators:

$$\begin{aligned} c_{j_a m_a}^\dagger c_{j_b m_b}^\dagger c_{j_c m_c} c_{j_d m_d} &= c_{j_a m_a}^\dagger (\delta_{j_b m_b, j_c m_c} - c_{j_c m_c} c_{j_b m_b}^\dagger) c_{j_d m_d} \\ &= \delta_{j_b j_c} \delta_{m_b m_c} c_{j_a m_a}^\dagger c_{j_d m_d} - c_{j_a m_a}^\dagger c_{j_c m_c} c_{j_b m_b}^\dagger c_{j_d m_d}, \end{aligned} \quad (108)$$

where the term containing $c_{j_a m_a}^\dagger c_{j_d m_d}$ is a charge-changing operator and can be ignored.

Inserting (108) into (107) and applying the definition (105),

$$\begin{aligned}
& \sum_M A_{JM}^\dagger(ab) A_{JM}(cd) \\
&= \sum_M \sum_{K\mu} (-1)^{J+M+j_b-j_d+\mu} (2J+1) \begin{Bmatrix} j_a & j_b & J \\ j_d & j_c & K \end{Bmatrix} (-1)^{-j_c+m_c-j_d+m_d} \rho_{K\mu}(a\tilde{c}) \rho_{K-\mu}(b\tilde{d}) \\
&= \sum_{K\mu} (-1)^{J+j_b+j_c} (2J+1) \begin{Bmatrix} j_a & j_b & J \\ j_d & j_c & K \end{Bmatrix} (-1)^\mu \rho_{K\mu}(a\tilde{c}) \rho_{K-\mu}(b\tilde{d}),
\end{aligned} \tag{109}$$

where I applied the condition that $M = m_a + m_b = m_c + m_d$ and the general property that $(-1)^j = (-1)^{j+2n}$ when n is an integer. In the second equality the constraint $\mu = m_a - m_c = -(m_b - m_d)$ eliminates the sum over M . To further simplify our notation, we define the dot product:

$$\begin{aligned}
\rho_K(a\tilde{c}) \cdot \rho_K(b\tilde{d}) &= \sum_{\mu} (-1)^K (2K+1)^{-1/2} (K\mu, K-\mu|00) \rho_{K\mu}(a\tilde{c}) \rho_{K-\mu}(b\tilde{d}) \\
&= \sum_{\mu} (-1)^{-\mu} \rho_{K\mu}(a\tilde{c}) \rho_{K-\mu}(b\tilde{d}),
\end{aligned} \tag{110}$$

where we applied the following identity for the case where we are coupling up to zero total angular momentum:²⁷

$$(K\mu, K-\mu|00) = (-1)^{K-\mu} (2K+1)^{-1/2}. \tag{111}$$

Thus the proton-neutron Hamiltonian can be written as

$$H_{pn} = \sum_{abcd} \sum_J V_J^{(pn)}(ab, cd) \sum_K (-1)^{J+j_b+j_c} (2J+1) \begin{Bmatrix} j_a & j_b & J \\ j_d & j_c & K \end{Bmatrix} \rho_K(a\tilde{c}) \cdot \rho_K(b\tilde{d}), \tag{112}$$

a coupling of the proton and neutron density matrices through a factor we define as:

$$W_K(ac, bd) \equiv \sum_J (-1)^{J+j_b+j_c} (2J+1) \begin{Bmatrix} j_a & j_b & J \\ j_d & j_c & K \end{Bmatrix} V_J^{(pn)}(ab, cd). \tag{113}$$

Our Hamiltonian is now in a form that can be recognized as potential matrix elements

$W_K(ac, bd)$ times one-body density operators $\hat{\rho}_K(a\tilde{c}) \cdot \hat{\rho}_K(b\tilde{d})$:

$$H_{pn} = \sum_{abcd} \sum_K W_K(ac, bd) \hat{\rho}_K(a\tilde{c}) \cdot \hat{\rho}_K(b\tilde{d}). \tag{114}$$

MATRIX ELEMENTS

Matrix elements can now be computed in our basis of coupled proton-neutron states using the above form of the Hamiltonian expressed in terms of density operators. Our full Hamiltonian is

$$H = H_p + H_{pp} + H_n + H_{nn} + H_{pn} \quad (115)$$

and the basis states are $|J_p^{\pi_p}, \alpha_p, J_n^{\pi_n}, \beta_n|J^\pi\rangle$.

The proton-only and neutron-only terms have matrix elements defined as

$$\langle J_p, \pi_p, \alpha_p | H_p + H_{pp} | J_p, \pi_p, \alpha_p \rangle \equiv h^{J_p^{\pi_p}}(\alpha'_p, \alpha_p) \quad (116)$$

and

$$\langle J_n, \pi_n, \alpha_n | H_n + H_{nn} | J_n, \pi_n, \alpha_n \rangle \equiv h^{J_n^{\pi_n}}(\beta'_n, \beta_n) \quad (117)$$

These are the single species operators whose matrix elements will be found as solutions from BIGSTICK.

$$\begin{aligned} (H_p + H_{pp})|J_p, \pi_p, \alpha_p\rangle &= E(\alpha_p)|J_p, \pi_p, \alpha_p\rangle \text{ and,} \\ (H_n + H_{nn})|J_n, \pi_n, \alpha_n\rangle &= E(\alpha_n)|J_n, \pi_n, \alpha_n\rangle. \end{aligned} \quad (118)$$

Thus we have:

$$\begin{aligned} h^{J_p^{\pi_p}} &= \delta_{a'_p a_p} E(\alpha_p) \text{ and,} \\ h^{J_n^{\pi_n}} &= \delta_{b'_n b_n} E(\alpha_n), \end{aligned} \quad (119)$$

which contribute:

$$\delta_{J'_n J_n} \delta_{J'_p J_p} \left(\delta_{\beta'_n \beta_n} h^{J_p}(\alpha'_p, \alpha_p) + \delta_{\alpha'_p \alpha_p} h^{J_n}(\beta'_n, \beta_n) \right). \quad (120)$$

The final term H_{pn} is a weighted sum of scalar products between two tensor operators of the form:

$$T(k) \cdot U(k) = \rho_K(a\tilde{c}) \cdot \rho_K(b\tilde{d}). \quad (121)$$

(See equation (114.) Since $\rho_K(a\tilde{c})$ acts only on protons, and $\rho_K(b\tilde{d})$ acts only on neutrons, these two operators commute, and can be computed in a coupled basis using a reduction to a product of operators in the uncoupled basis:²⁷

$$\begin{aligned} \langle j'_1 j'_2; J' M' | T(k) \cdot U(k) | j_1 j_2; J M \rangle = \\ (-1)^{j_1 + j'_2 + J} \delta_{J' J} \delta_{M' M} \left\{ \begin{matrix} J & j'_2 & j'_1 \\ k & j_1 & j_2 \end{matrix} \right\} \langle j'_1 | T(k) | j_1 \rangle \langle j'_2 | U(k) | j_2 \rangle \end{aligned} \quad (122)$$

In the case of (121), we will have our dependence on $\langle J_p'^{\pi_p}, \alpha'_p | \rho_k(a\tilde{c}) | J_p^{\pi_p}, \alpha_p \rangle$ and $\langle J_n'^{\pi_n}, \beta'_n | \rho_k(b\tilde{d}) | J_n^{\pi_n}, \beta_n \rangle$. These are just the proton and neutron density matrices represented in the basis of uncoupled proton and neutron states, respectively. Recalling that these uncoupled states are the eigenstates of the pure proton and pure neutron parts of the full Hamiltonian, these density matrices are density matrices produced by BIGSTICK when computing $H_p + H_{pp}$ and $H_n + H_{nn}$.

Then the proton-neutron Hamiltonian matrix elements are

$$\begin{aligned} \langle J_p'^{\pi_p}, \alpha'_p, J_n'^{\pi_n}, \beta'_n; J^\pi | \hat{H}_{pn} | J_p^{\pi_p}, \alpha_p, J_n^{\pi_n}, \beta_n; J^\pi \rangle = \\ \sum_{ac,bd} \sum_K W_K(ac, bd) (-1)^{J_p+J_n+J} \begin{Bmatrix} J & J'_n & J'_p \\ K & J_p & J_n \end{Bmatrix} \\ \langle J_p'^{\pi_p}, \alpha'_p | \rho_K(a\tilde{c}) | J_p^{\pi_p}, \alpha_p \rangle \langle J_n'^{\pi_n}, \beta'_n | \rho_K(b\tilde{d}) | J_n^{\pi_n}, \beta_n \rangle \end{aligned} \quad (123)$$

This matrix is then solved using techniques from linear algebra. In PNISM, the user can either select the included Lanczos algorithm to solve for low lying states or to use the full Householder diagonalization option using the routine SSYEV from the LAPACK²⁹ library, at the cost of increased run time.

The next major step is to calculate the one-body density matrices, used to calculate transition strengths. This is addressed in the next section.

ONE-BODY DENSITY MATRICES

A basic functionality of any configuration interaction code is the ability to calculate density matrices. A general one-body density matrix is defined by

$$\rho_k^{f,i}(ab) = \langle \Psi_f | [c_a^\dagger \otimes c_b]_k | \Psi_i \rangle, \quad (124)$$

which finds its use in the calculation of operator matrix elements

$$\langle \Psi_f | \hat{O} | \Psi_i \rangle = \sum_{ab} \rho_k^{f,i}(ab) \langle a | \hat{O} | b \rangle. \quad (125)$$

In order to calculate the density matrix elements between the eigenstates of the proton-neutron Hamiltonian, which are output from PNISM in the basis of coupled proton and neutron wavefunctions, we need to be able to write (124) in terms of the density matrices provided by BIGSTICK. These, however, are computed in the basis of pure proton and pure neutron wavefunctions. This section walks through the derivation of the one-body density

matrix elements for our eigenstates in terms of the one-body density matrices from the donor wavefunctions.

The matrix elements of a tensor product operator in a basis of coupled states are²⁷

$$\begin{aligned} & \langle j'_1 j'_2; J' | [\hat{T}_{k_1} \otimes \hat{U}_{k_2}]_K | j_1 j_2; J \rangle \\ &= [J'] [K] [J] \begin{Bmatrix} j'_1 & j_1 & k_1 \\ j'_2 & j_1 & k_2 \\ J' & J & K \end{Bmatrix} \langle j'_1 | \hat{T}_{k_1} | j_1 \rangle \langle j'_2 | \hat{U}_{k_2} | j_2 \rangle. \end{aligned} \quad (126)$$

If either \hat{T}_{k_1} or \hat{U}_{k_2} is the identity operator, as is the case for the one-body density matrices, then this expression further simplifies to

$$\begin{aligned} & \langle j'_1 j'_2; J' | [\hat{T}_{k_1}] | j_1 j_2; J \rangle \\ &= \delta_{j'_2 j_2} (-1)^{j'_1 + j_2 + J + K} [J'] [J] \begin{Bmatrix} j'_1 & J' & j_2 \\ J & j_1 & k \end{Bmatrix} \langle j'_1 | \hat{T}_k | j_1 \rangle \end{aligned} \quad (127)$$

and similarly for \hat{U}_{k_2} .

Thus we can find the proton density matrix elements in the coupled basis in terms of the density matrices in the uncoupled basis as

$$\begin{aligned} & \langle j'_\pi j'_\nu; J' | [\pi_a^\dagger \otimes \pi_c]_K | j_\pi j_\nu; J \rangle \\ &= \delta_{j'_\nu j_\nu} (-1)^{j'_\pi + j_\nu + J + K} [J'] [J] \begin{Bmatrix} j'_\pi & J' & j_\nu \\ J & j_\pi & k \end{Bmatrix} \langle j'_\pi | [\pi_a^\dagger \otimes \pi_c]_K | j_\pi \rangle \end{aligned} \quad (128)$$

The Kronecker- δ from the identity operator on the neutron space, and the orthogonality of the basis states. If more quantum numbers were included, more Kronecker- δ s would have to be added. Similarly, for the neutron density operator $[\nu_b^\dagger \otimes \nu_d]_K$ we have

$$\begin{aligned} & \langle j'_\pi j'_\nu; J' | [\nu_b^\dagger \otimes \nu_d]_K | j_\pi j_\nu; J \rangle \\ &= \delta_{j'_\pi j_\pi} (-1)^{j_\pi + j_\nu + J' + K} [J'] [J] \begin{Bmatrix} j'_\nu & J' & j_\pi \\ J & j_\nu & k \end{Bmatrix} \langle j'_\nu | [\pi_a^\dagger \otimes \pi_c]_K | j_\pi \rangle. \end{aligned} \quad (129)$$

Note that this is not as simple as exchanging π and ν .

Finally, to get the expression for the density matrix for our coupled-state solutions, recall that our states Ψ_f and Ψ_i in (124) are solutions to

$$\hat{H}|\Psi\rangle = E|\Psi\rangle \quad (130)$$

and are given in the basis of coupled proton-neutron states. Each state can be written as

$$|\Psi\rangle = \sum_{\alpha} c_{\alpha} |j_{\pi} j_{\nu}; J\rangle_{\alpha}. \quad (131)$$

Combining this expression (131) and the relation (128) with our definition (124), we obtain the desired result

$$\begin{aligned} \rho_k^{f,i}(\pi_a \pi_c) &= \langle \Psi_f | [\pi_a^{\dagger} \pi_c]_k | \Psi_i \rangle \\ &= \sum_{\alpha\beta} c_{\alpha}^f c_{\beta}^i \langle j_{\pi}^{\alpha} j_{\nu}^{\alpha}; J^f | [\pi_a^{\dagger} \pi_c]_k | j_{\pi}^{\beta} j_{\nu}^{\beta}; J^i \rangle \\ &= \sum_{\alpha\beta} c_{\alpha}^f c_{\beta}^i \delta_{j_{\nu}^{\alpha} j_{\nu}^{\beta}} (-1)^{j_{\pi}^{\alpha} + j_{\nu}^{\beta} + J^i + K} [J^f] [J^i] \begin{Bmatrix} j_{\pi}^{\alpha} & J^f & j_{\nu}^{\beta} \\ J^i & j_{\pi}^{\beta} & k \end{Bmatrix} \langle j_{\pi}^{\alpha} | [\pi_a^{\dagger} \pi_c]_K | j_{\pi}^{\beta} \rangle. \end{aligned} \quad (132)$$

The neutron one-body density matrix has identical structure.

This concludes the analytic discussions necessary to write the proton neutron interacting shell model code, PNISM. We have the expression for both the Hamiltonian matrix elements in terms of quantities which can be obtained from solutions from BIGSTICK (or any properly formatted results from an interacting shell model code), and the one-body density matrices which are used to compute transition rates. Although the code for computing one-body density matrices has been written and tested, we have yet to apply it. Equation (123) along with (113) and (132) are the actual equations coded up in PNISM.

CHAPTER 6

COMPUTATION

PNISM is a post processing code for BIGSTICK and relies on results from BIGSTICK in order to compute nuclear wavefunctions. Johnson wrote the majority of the subroutines responsible for reading in formatted results from BIGSTICK output files, as well as for constructing the basis. I aided in a few bug fixes in the modules responsible for reading in the density matrices (see "Challenges and Speedup"). I then wrote the majority of the code responsible for computing the proton-neutron-coupled-Hamiltonian H_{pn} , for solving the Hamiltonian, for computing the density matrices, and for writing the results to file. In this section I outline the flow of information and the algorithms and computations carried out. I leave out most of the theoretical details, as this is discussed in previous chapters, and focus on the computation.

The explicit proton-neutron formalism Hamiltonian is

$$H = H_p + H_{pp} + H_n + H_{nn} + H_{pn}. \quad (133)$$

BIGSTICK is used to solve $H_p + H_{pp}$ and $H_n + H_{nn}$ independently, before the PNISM runtime. Then PNISM reads in the following:

- The single particle orbit space
- The two-body matrix elements $\langle ab, JT | V | cd, JT \rangle$
- The energy levels and quantum numbers from both $H_p + H_{pp}$ and $H_n + H_{nn}$
- The density matrices from both $H_p + H_{pp}$ and $H_n + H_{nn}$, from solutions of different $M \equiv J_z$ values

After reading the all of the necessary resources, PNISM creates the basis by coupling the eigenstates of $H_p + H_{pp}$ and $H_n + H_{nn}$ up to states with good total angular momentum. Then, the array containing $W_K(ac, bd)$ is computed from the two-body matrix elements and with six-J symbols which are either computed on the fly or read in from a table stored on disk. Then, the largest portion of runtime takes place when the Hamiltonian matrix elements are computed using the diagonalized matrix elements of $H_p + H_{pp}$ and $H_n + H_{nn}$, the array

containing $W_K(ac, bd)$, the density matrices of $H_p + H_{pp}$ and $H_n + H_{nn}$, and again the six-J symbols. PNISM then diagonalizes the Hamiltonian matrix, thus solving the many-body Schrodinger equation. The resulting quantum numbers and eigenvectors are used to calculate the one-body density matrices and the results are written to a file in the same format as would be produced by BIGSTICK.

READING IN DENSITY MATRICES

PNISM must read in multiple solutions from BIGSTICK for the same proton/neutron configuration because BIGSTICK is an M-scheme code. A solution for a given M value will have some number of zero density matrix elements due to symmetries in the Clebsch-Gordan coefficients. Density matrices from BIGSTICK are actually reduced density matrices. A reduced matrix element of a tensor operator is a way to represent the matrix element of an operator without regard to the orientation in space. This is accomplished with the Wigner-Eckart theorem:²⁷ for a tensor operator $\hat{O}_K M$,

$$\begin{aligned} \langle J_f M_f | \hat{O}_{KM} | J_i M_i \rangle &= [J_f]^{-1} (J_i M_i K M | J_f M_f) \langle J_f | \hat{O}_K | J_i \rangle \\ &= (-1)^{J_f - M_f} \begin{Bmatrix} J_f & K & J_i \\ -M_f & M_K & M_i \end{Bmatrix} \langle J_f | \hat{O}_K | J_i \rangle, \end{aligned} \quad (134)$$

where $[j] \equiv \sqrt{2j+1}$ and the six-argument array is the six-J symbol. $\langle J_f | \hat{O}_K | J_i \rangle$ are the reduced density matrix elements of $\langle J_f M_f | \hat{O}_{KM} | J_i M_i \rangle$. A basic symmetry of vector coupling coefficients is²⁷

$$(j_a m_a j_b m_b | JM) = (-1)^{j_a + j_b - J} (j_b m_b j_a m_a | JM) \quad (135)$$

It can be shown by applying time reversal symmetries to equation (135) that²⁷

$$(j_a m_a j_b m_b | JM) = (-1)^{j_a + j_b - J} (j_a - m_a j_b - m_b | J - M). \quad (136)$$

Thus if $m_a = m_b = M = 0$ and $j_a + j_b - J$ is odd, the coefficient must be zero. This creates a problem for some of our reduced density matrices since we divide by this quantity. To recover the missing density matrix elements, we simply recompute $H_p + H_{pp}$ and $H_n + H_{nn}$ for another value of M . In practice, only $M = 0$ and $M = 1$ solutions are required to obtain nearly the entire solution. PNISM will only read in nonzero density matrix elements.

$M = 1$ basis states cannot have $J = 0$ total angular momentum (the total angular momentum can't be less than its z-component). Thus $M = 1$ solutions from BIGSTICK are

missing all $J = 0$ solutions. It is therefore necessary to read in $M = 0$ solutions first when setting up the basis. The overall phase of the density matrix elements first read in are taken to be the convention. An important obstacle that had to be overcome resulted from an ambiguity of quantum mechanics. When solving the Schrodinger equation, the overall sign of the wavefunction is not important, since it does not affect any observables. However, the relative phase between two wavefunctions is important, so care must be taken to establish self consistent phases. Because PNISM inputs solutions from BIGSTICK, the phase between two separate solutions, say, for two different $J_z \equiv M$ values (BIGSTICK is an M-scheme code) can differ. It is vital to check the relative phase between density matrices from different choices of M . Neglecting this will result in unforeseen cancellations and a failure to correctly recreate the Hamiltonian. After the initial density matrix that PNISM reads in, new density matrix elements for a given basis state combination are compared against density matrix elements that have already been read in. If an inconsistent phase is encountered, the read in is restarted for that basis state combination and the phase is adjusted accordingly.

SYMMETRIES

A number of basic symmetry relations were used to speed up calculations, the most obvious symmetry being the Hermiticity of the Hamiltonian matrix elements. After basic testing, only the diagonal and upper triangular portion of the Hamiltonian is computed independently. The remaining matrix elements are then copied over across the diagonal.

The proton-neutron potential factor $W_K(ac, bd)$ which appears in equation (113) has a similar symmetry:

$$W_K(ac, bd) = (-1)^{j_a + j_d - j_b - j_c} W_K(ca, db), \quad (137)$$

which is used to compute all iterations over a and c by computing only the $c \leq a$ matrix elements. Another but slightly less trivial method was used to compute the one-body density matrices. The one-body density matrices respect the so called time reversal symmetry:

$$\langle \Psi_f | [\hat{c}_a^\dagger \otimes \hat{c}_b]_k | \Psi_i \rangle = (-1)^{j_a - j_b + j_i - j_f} \langle \Psi_i | [\hat{c}_b^\dagger \otimes \hat{c}_a]_k | \Psi_f \rangle \quad (138)$$

This means that we only need to compute the upper triangular (in the a,b indices) elements of the one-body density matrices. The rest can be computed via the relation given in (138).

NUMERICAL METHODS

The primary eigensolver used in PNISM is SSYSEV from the LAPACK library.²⁹ PNISM has the option to either use SSYEV directly, or to use a custom Lanczos solver. The Lanczos solver is useful when only extremal eigenstates are sought. The Lanczos solver uses a straightforward lanczos iteration subroutine written by another graduate student, Ryan Zbikowski. The Lanczos method is discussed in Appendix A. In my implementation, I use an iterative process to incrementally increase the number of Lanczos iterations until some fixed number of eigenvalues converges. Convergence is measured by a somewhat crude criterion:

$$Crit = \frac{1}{N_{keep} - 1} \sum_{i=1}^{N_{keep}} |\lambda_i^{Current} - \lambda_i^{Previous}|. \quad (139)$$

Here, λ_i are the first N_{keep} eigenvalues produced by solving the Lanczos matrix. The process is said to have converged when the value of $Crit$ falls below some constant. In PNISM the value 0.001 is used. This is a similar convergence criterion to that used in BIGSTICK and empirical tests show that it converges to the correct values.

In some cases where the total dimension of the matrix is small compared to the number N_{keep} , the $Crit$ value will fail to become small enough, even when the number of lanczos iterations is maximum (equal to the dimension of the matrix). When this happens an flag is thrown and the code runs SSYEV instead.

CHALLENGES AND SPEEDUPS

Computing the matrix elements of the Hamiltonian in PNISM takes most of the overall runtime. Several actions were take to help reduce this runtime. Using the Unix profiling tool GPROF, I found that a large percentage of compute time was used in calling the function used to compute Six-J symbols, a function with six arguments and calls to other subfunctions within an external library. In order to reduce the time used computing six-J symbols, I wrote a small code to create a table of six-J tables called sj2i.f90. The code asks the user for six inputs, the six maximum value of angular momentum, J_{max} , to compute the six-J symbol for. The six-J symbols are then computed for all combinations of argument values from zero to Jmax and written to a file with the following format:

```
j1 j2 j3 j4 j5 j6 six-j(j1,j2,j3,j4,j5,j6)
```

In order to save disk space and I/O time, the file is written as an 'unformatted', non-ASCII file. Before any computation, PNISM reads the contents of the file into an array:

$$\begin{aligned} \text{sj2i_table}(j1+1, j2+1, j3+1, j4+1, j5+1, j6+1) \\ = \text{six-j}(j1, j2, j3, j4, j5, j6) \end{aligned}$$

At the time when this document was written, the entire Hamiltonian for all total J values is computed sequentially, and then solved afterward. This is a waste of memory since each total J Hamiltonian is independent and can be solved before the next is computed and committed to memory. A future project will be to solve each matrix as soon as it is computed. This should reduce the maximum memory requirements by approximately a factor equal to the total number of total-J values requested, i.e. if computing J-total from 0 to 10 then as much as one-tenth the total memory will be required with little cost to runtime.

CHAPTER 7

RESULTS

There are two classes of results discussed here: ground state energy convergence and excitation spectra of atomic nuclei. Existing interacting shell model codes such as BIGSTICK have errors with respect to experiment of around a few hundred keV. Since our interacting shell model PNISM is an approximation to these results found in BIGSTICK, and are bounded by the variational principle (see Appendix A.6), we expect the results computed by PNISM to converge to the results of BIGSTICK as the size of the basis is increase. Ground state energies are found to converge exponentially and monotonically with the size of the basis, and excitation spectra also converge to the results of BIGSTICK, although in a more sporadic and unpredictable way. This is because PNISM is a J-scheme code: we should expect that the excitation spectra for fixed-J to obey the variational principle, but a plot of low-lying excitations, having mixed J-values, will have non-monotonic convergence curves. This can be understood by realizing that as each fixed-J excitation spectra settles downward towards the energy of the untruncated basis, the gaps between ordered energy levels may grow or shrink as excitation spectra from different J values converge at different rates. This can be seen in the excitation plots at the end of the chapter.

Results demonstrate the exponential convergence of the ground state energy as a function of the number of states retained, for nuclei where a full diagonalization is possible even on a laptop. Results are given for sample nuclei in both the sd shell and the pf shell. When all of the states are retained, the results are exactly equal to those of BIGSTICK. Results also demonstrate the convergence of low-lying excitations in the sd and pf shells. When all of the states are retained, the results are exactly equal to those of BIGSTICK for all excitation levels. Qualitatively one can observe that $N > Z$ nuclei tend to converge faster than $N = Z$ nuclei.

In order to examine the convergence of the wavefunctions, we calculated the density matrices for nuclei in both model spaces. As expected, when all of the states are included, the results converge to those of BIGSTICK.

CAPSTONE CALCULATIONS

These calculations are meant to push PNISM to its limits to demonstrate its use. We study three nuclei, ^{56}Ni , ^{60}Ni and ^{64}Ge in the $(p_{1/2}, p_{3/2}, f_{5/2}, f_{7/2})$ model space. The M-scheme basis dimensions of these nuclei are compared in Table 7. The M-scheme dimensions of the proton Hamiltonian and the neutron Hamiltonian for these nuclei is shown in Table 8. (These are used by PNISM to build the J-scheme basis for nuclei in the $(p_{1/2}, p_{3/2}, f_{5/2}, f_{7/2})$ model space.)

Table 7. M-scheme Dimensions for Select Nuclei in the $(p_{1/2}, p_{3/2}, f_{5/2}, f_{7/2})$ Model Space

Nuclide	Val. protons	Val. neutrons	M-scheme dim.	Ground state E [MeV]
^{56}Ni	8	8	1.09×10^9	-72.56190
^{60}Ni	8	12	1.09×10^9	-80.26105
^{64}Ge	12	12	1.09×10^9	-98.81734

Table 8. Dimensions for Proton and Neutron Hamiltonians

Hamiltonian	Val. protons	Val. neutrons	M-scheme dim.
$\hat{H}_{neutron}$	0	8	12022
\hat{H}_{proton}	8	0	12022
\hat{H}_{proton}	12	0	12022
$\hat{H}_{neutron}$	0	12	12022

When computing the excitation spectra of these nuclei and limiting ourselves to 16 GB of memory, we were able to keep up to 200 of the 12022 available eigenstates of the pure proton and pure neutron Hamiltonians. Exact dimensions of the truncated J-scheme basis are given for ^{56}Ni in Table 9. (As a function of number N of proton and neutron wavefunctions retained for coupled J-scheme basis using M-scheme solutions in the $(p_{1/2}, p_{3/2}, f_{5/2}, f_{7/2})$ model space. $N_{max} = 12022$. J-scheme dimension is the size of the Hamiltonian for fixed J . Absolute error and percent error are computed relative to M-scheme solution from BIGSTICK.) The same data for ^{60}Ni is found in Table 10. (As a function of number N of

proton and neutron wavefunctions retained for coupled J-scheme basis using M-scheme solutions in the $(p_{1/2}, p_{3/2}, f_{5/2}, f_{7/2})$ model space. $N_{max} = 12022$. J-scheme dimension is the size of the Hamiltonian for fixed J . Absolute error and percent error are computed relative to M-scheme solution from BIGSTICK.) Computing the matrix elements of the Hamiltonian for a calculation of a handful low-lying states requires several sets of bases for different J values.

Table 9. ^{56}Ni Ground State Energy and J-scheme Dimensions

N	J-scheme dim.	Ground state E [MeV]	Abs. error	Perct. error
10	22	-70.558	2.004	2.76
50	384	-71.957	0.6049	0.833
100	1408	-72.010	0.5519	0.761
200	5128	-72.195	0.3669	0.506
400	19838	-72.318	0.2439	0.336
600	43912	-72.424	0.1383	0.191

Table 10. ^{60}Ni Ground State Energy and J-scheme Dimensions

N	J-scheme dim.	Ground state E [MeV]	Abs. error	Perct. error
10	20	-76.731	3.5400	4.398
50	412	-78.839	1.4221	1.778
100	1477	-79.000	1.2611	1.571
200	5424	-79.408	0.8531	1.063
400	20459	-79.869	0.3921	0.4885
600	45086	-80.046	0.2151	0.2679

HEAVY NUCLEI

In the future we would like to target a number of specific nuclei relevant to important experimental physics. In this section I will provide estimates for the dimension of these problems in the M-scheme, and the dimensions of the proton and neutron Hamiltonians that would need to be solved in their place in order to construct the J-scheme basis.

Some experimental searches for non-baryonic dark matter involve collisions with heavy nuclei such as ^{131}Xe , and require detailed nuclear structure calculations.³ Xe isotopes, as well as the Cs isotopes for studying the nuclear anapole moment, can both be computed in the model space with single particle orbits:

$$g_{7/2}, d_{5/2}, d_{3/2}, s_{1/2}, h_{11/2}, \quad (140)$$

which will be referred to as the GCN5082 model space, after the name of the interaction file used for this configuration space. The M-scheme dimension of ^{133}Cs and ^{131}Xe are both around 1.98×10^8 . ^{131}Xe has 77 neutrons and 54 protons, while ^{133}Cs has 78 neutrons and 55 protons. The fact that these both have an unequal number of protons and neutrons is encouraging; our J-scheme approximation is predicted to be well suited for such nuclei.

The origin of the matter-antimatter symmetry violation may be due to CP-violation,⁴ and one approach to investigating the source of CP-violation is through the permanent electric dipole moments of certain nuclei such as ^{199}Hg .⁵ Model spaces for nuclei with such a high mass number do not yet exist, and we would have to create the interaction for it. Nonetheless we can still predict the M-scheme dimensions of the proton and the neutron parts of the Hamiltonian. ^{199}Hg has 80 protons and 119 neutrons. This means that the proton Hamiltonian will most likely be computed in the GCN5082 model space (see equation (140)), and the neutron Hamiltonian would have to be computed in a new shell model space. This could be defined by the set of orbitals

$$1h_{9/2}, 2f_{7/2}, 2f_{5/2}, 3p_{3/2}, 3p_{1/2}, 1i_{13/2}, \quad (141)$$

which corresponds to between 82 and 126 nucleons. (The next pair of consecutive magic numbers.)

Table 11 contains estimates for the M-scheme dimension of the Hamiltonian for these nuclei of interest. It also provides estimates for the M-scheme dimension of the proton Hamiltonian and the neutron Hamiltonian that would need to be solved in order to compute the J-scheme basis for PNISM. These are orders of magnitude smaller than the full interaction's dimension. The estimated dimension of the M-scheme proton Hamiltonian for ^{199}Hg corresponds to a calculation in the GCN5082 space, while the neutron Hamiltonian is estimated for the new single-particle space defined by (141).

Table 11. Estimated Dimensions of Target Heavy Nuclei.

Nucleus	Space	M-scheme dim.	Proton dim.	Neutron dim.
^{133}Cs	GCN5082	1.98×10^8	1500	7500
^{131}Xe	GCN5082	1.98×10^8	1500	7500
^{199}Hg	Unknown	Unknown	36	1.04×10^6

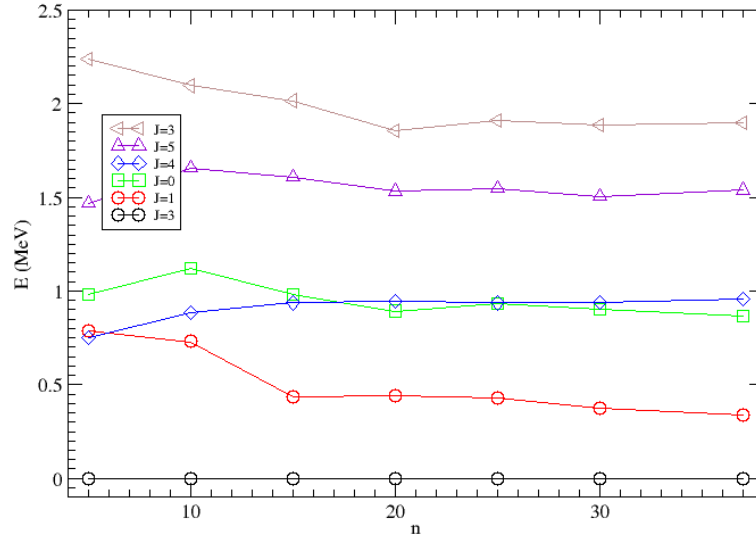


Figure 14. ^{22}Na low-lying excitation spectra as a function of n , the number of eigenstates retained from the pure proton and pure neutron interactions used to form the basis. Here the maximum value of n is $n = 37$, when the entire basis is retained.

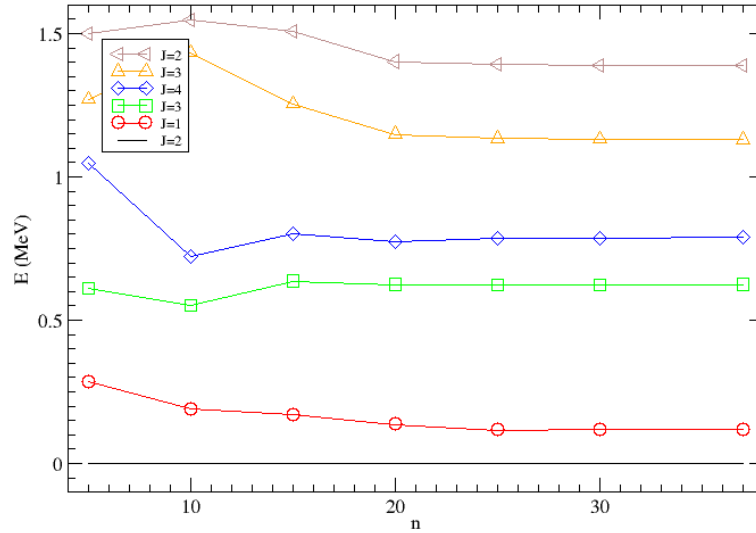


Figure 15. ^{28}Na low-lying excitation spectra as a function of the number of retained n . $n_{max} = 37$. Notice that ^{28}Na converges faster than ^{22}Na , while having the same basis dimensions.

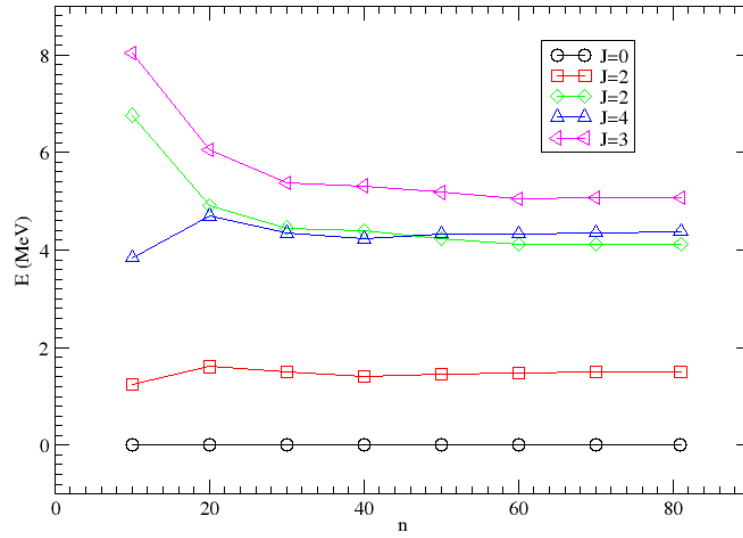


Figure 16. ^{24}Mg low-lying excitation spectra. Symbols as in Figure 14. Here $n_{max} = 81$.

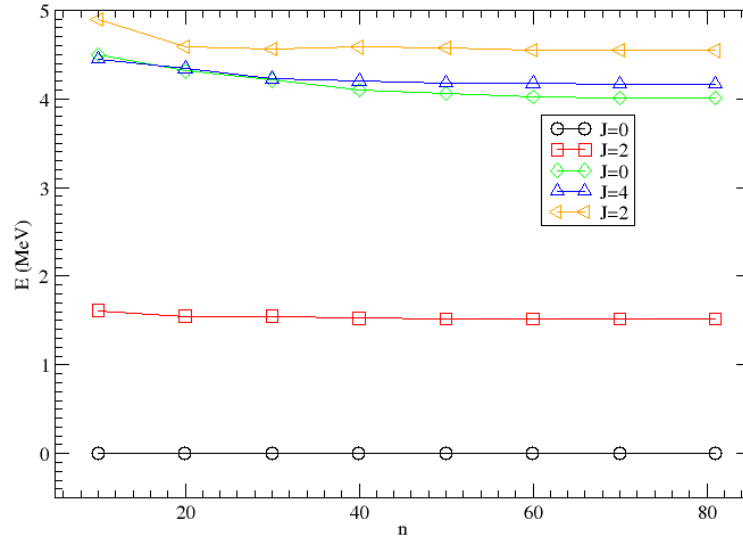


Figure 17. ^{28}Mg low-lying excitation spectra. Symbols as in Figure 14. $n_{max} = 81$ is the same as for ^{24}Mg , but energies converge faster for ^{28}Mg .

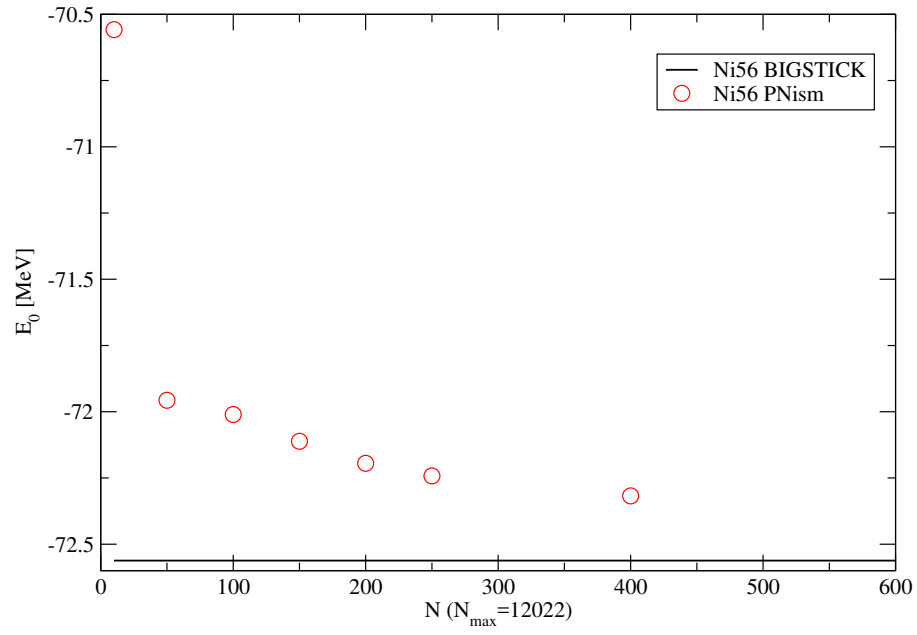


Figure 18. ^{56}Ni ground state energy convergence relative to complete basis wavefunction.

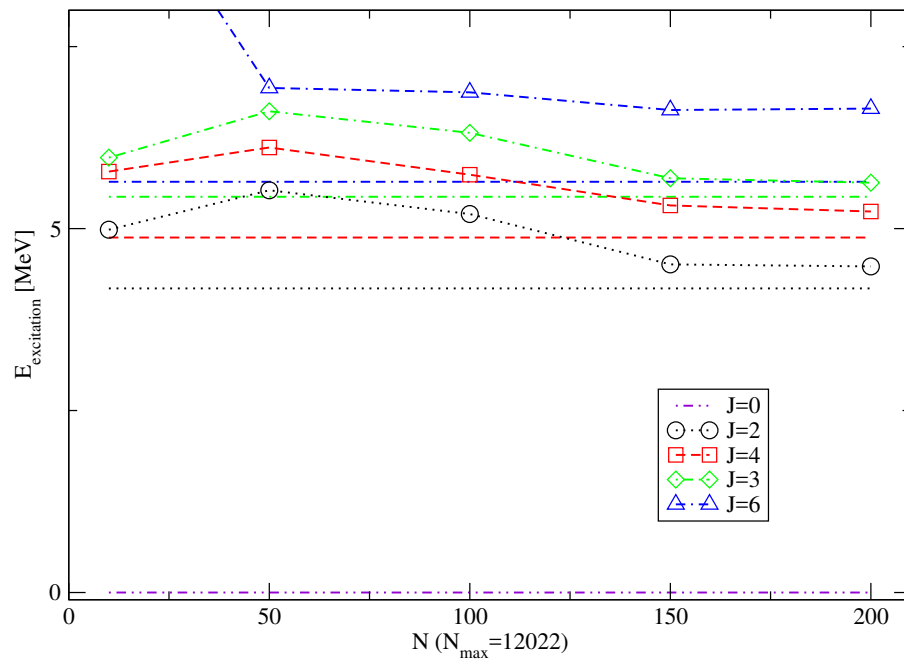


Figure 19. ^{56}Ni low-lying excitation spectra. Unmarked curves are results from M-scheme calculation.

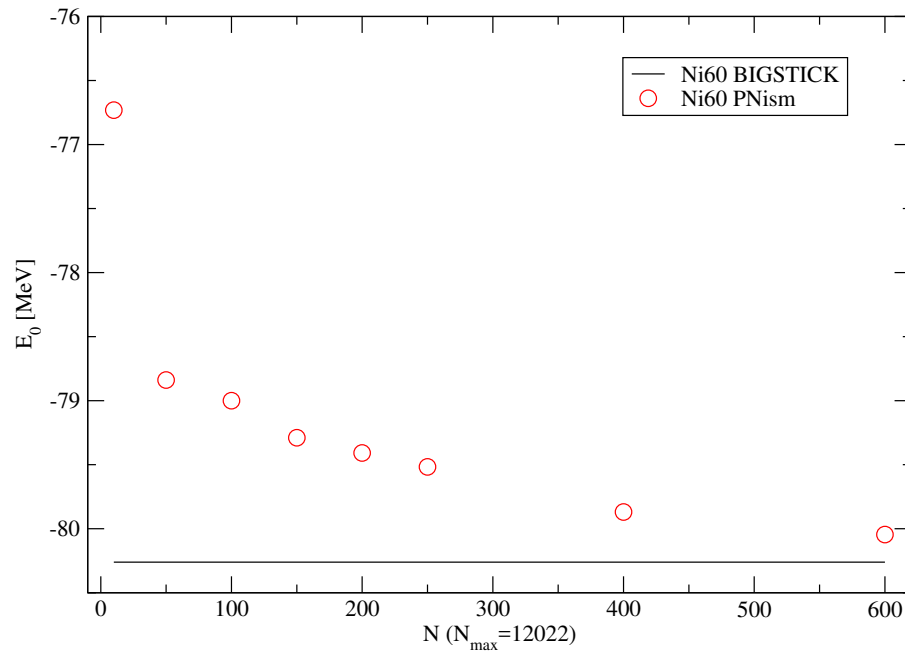


Figure 20. ^{60}Ni ground state energy convergence relative to complete basis wavefunctions as a function of the number of single-species basis states retained.

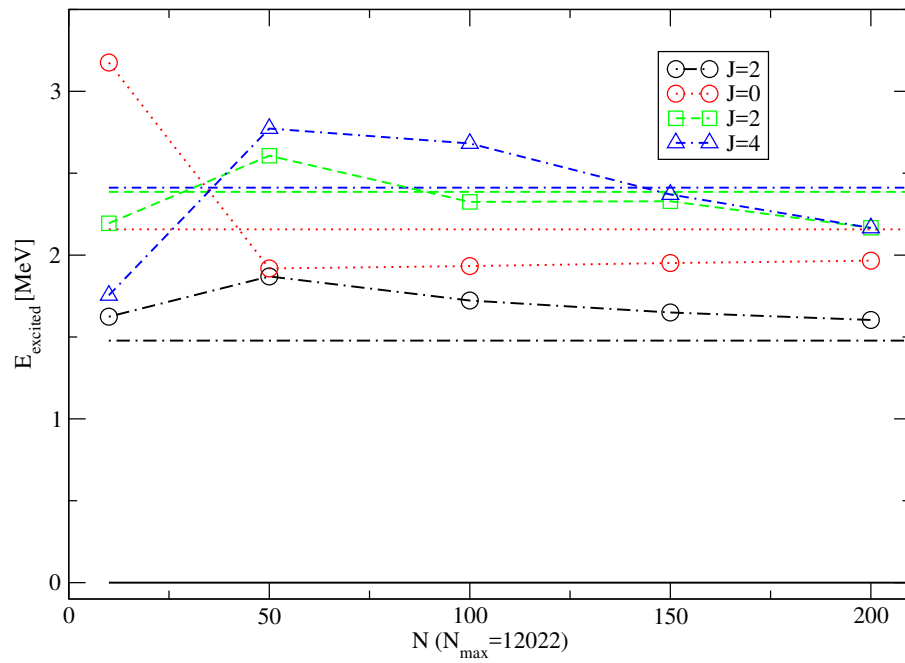


Figure 21. ^{60}Ni low-lying excitation spectra. Unmarked curves are results from M-scheme.

CHAPTER 8

CONCLUSION AND FUTURE WORK

This thesis was a study of proton-neutron entanglement entropy and the presentation of a new interaction shell model code, PNISM. It was shown that the proton-neutron entanglement entropy is inversely correlated with the isospin of a atomic nuclei. This hypothesis was further supported by a decomposition of nuclear wavefunctions into pure proton and pure neutron eigenstates, which fall off exponentially. The fact that nuclei with greater isospin appear to have weaker proton-neutron coupling suggests that heavier nuclei with high isospin could be computed with even greater efficiency using this truncation scheme.

We wrote a J-scheme interacting shell model code which takes proton wavefunctions and neutron wavefunctions and creates a truncated basis of coupled proton and neutron wavefunctions. The nuclear Hamiltonian is computed in this basis and solved using standard numerical techniques. The ground state energy and wavefunctions converge exponentially to those of the full model space. The results for three nuclei in the $(p_{1/2}, p_{3/2}, f_{5/2}, f_{7/2})$ model space, which would normally require a supercomputer to solve, were computed using PNISM running on a laptop. Results are not satisfactory and further research will need to be done to improve convergence. Eventually we would like be able to compute nuclei with full model space dimensions in the billions using truncated model spaces in PNISM; however we are still working on some bugs to do with model spaces with more than one parity.

In the future we will need to make changes to the code to improve convergence. The model presented here is the simplest version in that basis states are selected from the lowest eigenstates of the proton and neutron Hamiltonians. This could be improved by introducing effective single-particle energies to account for the contribution from the remaining states which were left out, perhaps through some mean-field approximation.

In the current version, PNISM computes the entire set of Hamiltonian matrix elements before diagonalizing. Memory utilization could be greatly improved by diagonalizing the

Hamiltonian after completing each value of total angular momentum. This is possible since PNISM is a J-scheme code; matrix elements between states with different total J are independent. Here is a pseudo-code depiction of the current procedure:

```
DO J = JMIN, JMAX
    COMPUTE <AB,J| H |CD,J>
END DO

DO J = JMIN, JMAX
    DIAGONALIZE <AB,J| H |CD,J>
END DO

DEALLOCATE <AB,J| H |CD,J>
```

The problem being that this requires storing the entire Hamiltonian in memory before diagonalizing and writing to disk the much smaller set of truncated eigenstates and quantum numbers. If instead we use the following procedure:

```
DO J = JMIN, JMAX
    COMPUTE <AB,J| H |CD,J>
    DIAGONALIZE <AB,J| H |CD,J>
    DEALLOCATE <AB,J| H |CD,J>
END DO
```

then we can expect a reduction in the total memory resources required by a factor that scales like the number of J states required. While simple in principle, this will require a nontrivial restructuring of the code.

This reorganization of the code would also be compatible with a hybrid implementation of MPI³⁰ and openMP.³¹ MPI is a distributed memory message passing interface commonly used for parallelization. MPI will be called to distribute iterations of the loop over J values to various nodes of a cluster. Each node, being assigned some allotment of work, will create numerous threads using openMP, a shared memory multi-processing programming interface. If only one node is available, then creation of openMP threads will be preferred.

REFERENCES

- ¹ A. Faessler, J. of Phys.: Conference Series **337**, 012065 (2012).
- ² B. A. Brown, M. Horoi, and A. Sen'kov, Phys. Rev. Lett. **113**, 1 (2014).
- ³ V. Bednyakov and F. Simkovic, Phys. Part. Nucl. **36**, 131 (2005).
- ⁴ A. Sakhorav, JETP Lett. **5**, 24 (1967).
- ⁵ L. Willmann and K. Jungmann, Ann. Phys. (Berl.) **528**, 108 (2015).
- ⁶ W. C. Haxton, E. M. Henley, and M. J. Musolf, Phys. Rev. Lett. **63**, 949 (1989).
- ⁷ W. C. Haxton, C. P. Liu, and M. J. Ramsey-Musolf, Phys. Rev. C **65**, 045502 (2002).
- ⁸ C. W. Johnson, W. E. Ormand, and P. G. Krastev, Comp. Phys. Comm. **184**, 2761 (2013).
- ⁹ B. C. Hall, *Quantum Theory for Mathematicians* (Springer, New York, 2013).
- ¹⁰ J. M. Eisenberg and W. Greiner, *Microscopic Theory of the Nucleus* (North-Holland Publishing Company, Amsterdam, 1972).
- ¹¹ P. A. M. Dirac, Proc. R. Soc. Lond. A **112**, 661 (1926).
- ¹² N. Jeevanjee, *An Introduction to Tensors and Group Theory for Physicists* (Springer, Switzerland, 2011).
- ¹³ S. S. M. Wong, *Introductory Nuclear Physics* (Wiley-VCH, Weinheim, 2004).
- ¹⁴ A. Fetter and J. Walecka, *Quantum Theory of Many-Particle Systems* (McGraw-Hill, New York, 1971).
- ¹⁵ C. W. Johnson, W. E. Ormand, K. S. McElvain, and H. Shan, *BIGSTICK: A flexible configuration-interaction shell-model code* (Department of Physics, San Diego State University, 2018).
- ¹⁶ P. J. Brussaard and P. W. M. Glaudemans, *Shell-model Applications in Nuclear Spectroscopy* (North-Holland Publishing Company, Amsterdam, 1977).
- ¹⁷ E. Segre, *Nuclei and Particles* (Benjamin/Cummings Publishing Company, Reading, Massachusetts, 1977).
- ¹⁸ K. Heyde, *Basic Ideas and Concepts in Nuclear Physics* (Institute of Physics Publishing, London, 1994).
- ¹⁹ B. A. Brown and W. A. Richter, Phys. Rev. C **74**, 034315 (2006).
- ²⁰ T. C. S. E. W. Group, *Data Formats and Procedures for the Evaluated Nuclear Data File ENDF-6* (National Nuclear Data Center, Brookhaven National Laboratory, 1995).
- ²¹ T. Papenbrock and D. J. Dean, Phys. Rev. C **67**, 051303 (2003).
- ²² T. Papenbrock, A. Juodagalvis, and D. J. Dean, Phys. Rev. C **69**, 024312 (2004).

- ²³ T. Papenbrock and D. J. Dean, J. Phys. G: Nucl. Part. Phys. **31**, S1377 (2005).
- ²⁴ W. H. Press, S. A. Teukolsky, W. T. Vetterling, and B. P. Flannery, *Numerical Recipes in Fortran 77* (Cambridge University Press, Cambridge, 1992).
- ²⁵ E. Caurier, G. Martínez-Pinedo, F. Nowacki, A. Poves, and A. P. Zuker, Rev. Mod. Phys. **77**, 427 (2005).
- ²⁶ P. Ring and P. Schuck, *The Nuclear Many-Body Problem* (Springer-Verlag, New York, 1980).
- ²⁷ A. R. Edmonds, *Angular Momentum in Quantum Mechanics* (Princeton University Press, Princeton, NJ, 1957).
- ²⁸ A. deShalit and H. Feshbach, *Theoretical Nuclear Physics, Volume I: Nuclear Structure* (John Wiley and Sons, INC., New York, 1974).
- ²⁹ F. Anderson *et al.*, *LAPACK Users' Guide* (Society for Industrial and Applied Mathematics, Philadelphia, 1999).
- ³⁰ M. P. I. Forum, *MPI: A Message-Passing Interface Standard*, (University of Tennessee, 2012).
- ³¹ OpenMP Board, *OpenMP Application Programming Interface* (OpenMP Architecture Review Board, 2015).
- ³² R. Shankar, *Principles of Quantum Mechanics* (Springer, New York, 1994).
- ³³ J. Cullum and R. A. Willoughby, J. Comp. and App. Math. **12**, 37 (1985).

APPENDIX A

Supplementary Notes

Supplementary Notes

VECTOR COUPLING COEFFICIENTS

Vector coupling coefficients, commonly referred to as Clebsch-Gordan coefficients³² are simply the coefficients of an expansion of a coupled angular momentum state with fixed total J in a basis of coupled states $|j_1 m_1, j_2 m_2\rangle \equiv |j_1 m_1\rangle \otimes |j_2 m_2\rangle$. That is to say, in the expansion

$$|j_1 j_2; JM\rangle = \sum_{m_1 m_2} |j_1 m_1, j_2 m_2\rangle \langle j_1 m_1, j_2 m_2 | j_1 j_2; JM\rangle, \quad (142)$$

the inner products $\langle j_1 m_1, j_2 m_2 | j_1 j_2; JM\rangle$ are the vector coupling coefficients. This are often written as

$$(j_1 m_1 j_2 m_2 | JM) \equiv \langle j_1 m_1, j_2 m_2 | j_1 j_2; JM\rangle \quad (143)$$

so that

$$|j_1 j_2; JM\rangle = \sum_{m_1 m_2} (j_1 m_1 j_2 m_2 | JM) |j_1 m_1, j_2 m_2\rangle. \quad (144)$$

3-J SYMBOL

An alternative to the vector-coupling coefficients are the so called three-J symbols (3-j symbols). They are defined in terms of the vector coupling coefficients for the coupling of three angular momenta:²⁷

$$\begin{Bmatrix} j_1 & j_2 & j_3 \\ m_1 & m_2 & m_3 \end{Bmatrix} \equiv (-1)^{j_1-j_2-m_2} (2j_2+1)^{-1/2} (j_1 m_1 j_2 m_2 | j_1 j_2 j_3 - m - 3). \quad (145)$$

6-J SYMBOLS AND 9-J SYMBOLS

Six-J and Nine-9 symbols are generalizations of vector coupling coefficients which often appear in calculations involving complex angular momentum algebra. I refer the reader to Edmonds²⁷ for a complete description.

SINGULAR VALUE DECOMPOSITION

A singular value decomposition is a eigenvalue decomposition, generalized to non-square non-symmetric matrices. The method of singular value decomposition comes

from a theorem which tells us that any $M \times N$ matrix A with $M \geq N$ can be written as the product of an $M \times N$ column-orthogonal matrix U , an $N \times N$ diagonal matrix W with positive or zero elements (the singular values), and the transpose of an $N \times N$ orthogonal matrix V .²⁴ That is,

$$A_{M \times N} = U_{M \times N} W_{N \times N} V_{N \times N}^T \quad (146)$$

or in matrix notation,

$$A_{ij} = \sum_{a=1}^N U_{ia} \sum_{b=1}^N W_{ab} V_{jb} \quad (147)$$

Which, for the case where $M = N$, simply states that we can write a matrix A as a unitary transformation of a diagonal matrix containing the eigenvalues of A :

$$A_{ij} = \sum_{ab} U_{ia} W_{ab} U_{jb}. \quad (148)$$

LANCZOS METHOD

This is an overview of the Lanczos method³³ used in this research. The Lanczos Algorithm is used to obtain the extremal eigenvalues of an $n \times n$ Hermitian matrix in $m < n$ linear operations. This is done by transforming the Hermitian matrix into a truncated tridiagonal matrix containing the extremal eigenvalues,

$$T = V^\dagger H V \quad (149)$$

We begin with an $n \times n$ real-symmetric matrix H and a fixed number $k \ll n$ of iterations to carry out. Generate a random normalized vector $v(0)$ of dimension n and carry out the following procedure:

FOR all Lanczos iterations

$$|w\rangle = H|v(i)\rangle$$

$$a(i) = \langle v(i) | w \rangle$$

! Orthogonalize against initial vector

$$|w\rangle = |w\rangle - a(i)|v(i)\rangle$$

IF ($i > 1$), FOR all previous iterations

! Orthogonalize against prior vectors

$$|w\rangle = |w\rangle - \langle v(j) | w \rangle |v(j)\rangle$$

$$b(i) = |w|$$

$$|v(i+1)\rangle = |w\rangle / b(i)$$

After k iterations, the vectors $v(i)$ form the transformation matrix V and a and b contain the diagonal and subdiagonal elements of the tridiagonal matrix T .

This algorithm can be used to extract the extremal eigenvalue and eigenvectors of H . By diagonalizing T , one can find $Tx = \lambda x$ where x and λ are the eigenvectors and eigenvalues of T . H and T are *similar* matrices and therefore have the same eigenvalues. Simultaneously $H\psi = \lambda\psi$ and $Tx = \lambda x$, so

$$\begin{aligned} V^\dagger H V x &= \lambda x \\ V V^\dagger H V x &= V \lambda x \\ H V x &= \lambda V x, \end{aligned} \tag{150}$$

thus $\psi = Vx$ tells us how to obtain the eigenvectors of H given the eigenvectors of T .

VARIATIONAL PRINCIPLE

The Variational Principle is an extremely useful theorem in quantum mechanics as it is the basis of many methods. The principle states that the expectation value of the Hamiltonian in any state is greater than or equal to the expectation value of the Hamiltonian in the ground state. Suppose we have a Hamiltonian \hat{H} and an arbitrary state $|\phi\rangle$ both in some Hilbert space H . Because \hat{H} is Hermitian, we are guaranteed that it has a complete set of eigenvectors and eigenvalues, $|\psi\rangle_i$ and E_i . Suppose that the lowest eigenstate has some, perhaps unknown, eigenvalue E_0 . The Variational Principle is that the expectation value of \hat{H} in the state $|\phi\rangle$ is

$$\frac{\langle \phi | \hat{H} | \phi \rangle}{\langle \phi | \phi \rangle} \geq E_0. \tag{151}$$

This is straightforward to prove since we can always write $|\phi\rangle = \sum_i c_i |\psi\rangle_i$. Then equation (1) can be written

$$\begin{aligned}
 \frac{\langle\phi|\hat{H}|\phi\rangle}{\langle\phi|\phi\rangle} &= \frac{\sum_j c_j^* \langle\psi|_j \hat{H} \sum_i c_i |\psi\rangle_i}{\sum_j c_j^* \langle\psi|_j \sum_i c_i |\psi\rangle_i} \\
 &= \frac{\sum_{j,i} c_j^* c_i \langle\psi|_j \hat{H} |\psi\rangle_i}{\sum_{j,i} c_j^* c_i \delta_{i,j}} \\
 &= \frac{1}{\sum_i |c_i|^2} \sum_{j,i} c_j^* c_i E_i \delta_{j,i} \\
 &= \frac{1}{\sum_i |c_i|^2} \sum_j |c_j|^2 E_j
 \end{aligned} \tag{152}$$

Since $E_0 \leq E_i$ for all i , each term satisfies $|c_j|^2 E_0 \leq |c_j|^2 E_j$ and

$$\frac{1}{\sum_i |c_i|^2} \sum_j |c_j|^2 E_j \geq \frac{1}{\sum_i |c_i|^2} E_0 \sum_j |c_j|^2 \geq E_0. \tag{153}$$

This inequality allows us to propose a model wavefunction and have the guarantee that our ground state will be bounded.

APPENDIX B

Sample Density Matrix Files

Sample Density Matrix Files

Here I have provided some redacted density matrix files to provide some context for the discussion given on reading in density matrices. The following are data from input files to be read into PNISM. The format of the density matrix files is

$$\langle Final State | [\pi_a^\dagger \pi_c]_{J_t} | Initial State \rangle \quad (154)$$

These particle density matrix files are used for calculating ^{20}Ne in the sd model space with an inert ^{16}O core. This means that there are two valence protons and two valence neutrons. This first file contains the excitation spectra and density matrices for a nuclei with two protons and zero neutrons with $M = J_z = 0$.

```

BIGSTICK Version 7.8.1 Sept 2017
single-particle file = sd
          2          0    <--- #protons, #neutrons
          0 +          <--- Jz, parity
Time to compute jumps :    9.9999993108212948E-004
Time to compute jumps :    0.000000000000000000
State      E      Ex      J      T
   1    -11.77906   0.00000   -0.000   1.000
   2     -9.84945   1.92961    2.000   1.000
   3     -8.37591   3.40315    4.000   1.000
...
Initial state #    2 E =   -9.84945 2xJ, 2xT =    4    2
Final state  #    4 E =   -7.56341 2xJ, 2xT =    4    2
Jt =   0, proton      neutron
   1    1  -0.01892   0.00000
   2    2   0.45231   0.00000
   3    3  -0.75667   0.00000
Jt =   2, proton      neutron

```

```

1      1  -0.01948  0.00000
1      2   0.04273  0.00000
1      3  -0.00230  0.00000
2      1  -0.05930  0.00000
2      2  -0.65142  0.00000
2      3   0.40773  0.00000
3      1  -0.03520  0.00000
3      2  -0.71134  0.00000
Jt =   4, proton      neutron
1      2   0.06297  0.00000
2      1  -0.13163  0.00000
2      2   0.08321  0.00000
...

```

This second file contains the excitation spectra and density matrices for a nuclei with two protons and zero neutrons with $M = J_z = 1$. Notice that the states number labels do not match up between the two files. The $M = J_z = 1$ results are missing states with $J = 0$; you cannot have total angular momentum less than the z-component of the angular momentum. Also notice that density matrix elements between the same states (identified by E , J , and T quantum numbers) are identical up to a phase. The $M = J_z = 1$ density matrix file also has the entire set of J_t quantum numbers for a given initial and final state while the $M = J_z = 1$ density matrix file is missing odd J_t quantum numbers. Both solutions are required by PNISM to obtain the entire density matrix.

BIGSTICK Version 7.8.1 Sept 2017

single-particle file = sd

2 0

2 +

Time to compute jumps : 1.0000001639127731E-003

Time to compute jumps : 0.000000000000000000

State	E	Ex	J	T
1	-9.84945	0.00000	2.000	1.000
2	-8.37591	1.47354	4.000	1.000

```

      3      -7.56341      2.28605      2.000      1.000
...
Initial state #      1 E =      -9.84945 2xJ, 2xT =      4      2
Final state      #      3 E =      -7.56341 2xJ, 2xT =      4      2

Jt =   0, proton      neutron
      1      1      0.01892      0.00000
      2      2     -0.45231      0.00000
      3      3      0.75667      0.00000
Jt =   1, proton      neutron
      1      1      0.01886      0.00000
      1      2     -0.03956      0.00000
      1      3      0.02182      0.00000
      2      1      0.00724      0.00000
      2      2      0.04334      0.00000
      3      1     -0.03337      0.00000
      3      3     -0.31605      0.00000
Jt =   2, proton      neutron
      1      1      0.01948      0.00000
      1      2     -0.04273      0.00000
      1      3      0.00230      0.00000
      2      1      0.05930      0.00000
      2      2      0.65142      0.00000
      2      3     -0.40773      0.00000
      3      1      0.03520      0.00000
      3      2      0.71134      0.00000
Jt =   3, proton      neutron
      1      1      0.02028      0.00000
      1      2     -0.03333      0.00000
      2      1      0.13226      0.00000
      2      2      0.75618      0.00000
      2      3      0.17724      0.00000
      3      2     -0.29377      0.00000

```

Jt =	4,	proton	neutron
1	2	-0.06297	0.00000
2	1	0.13163	0.00000
2	2	-0.08321	0.00000

...